Schistosoma mansoni infection induces long-lived sex-specific metabolic reprogramming of the myeloid lineage

Diana Cortes-Selva[1], Lisa Gibbs[1], J. Alan Maschek [5,6], Tyler Van Ry[3,5], Bartek Rajwa[2], James E. Cox[3,5], Eyal Amiel[4], Keke C. Fairfax [1]

[1] Department of Pathology, Division of Microbiology and Immunology, University of Utah, Salt Lake City UT, 84112
[2] Bindley Bioscience Center, Purdue University, West Lafayette IN, 47907
[3] Department of Biochemistry, University of Utah, Salt Lake City UT, 84112
[4] Department of Biomedical and Health Sciences, University of Vermont, Burlington, VT 05405
[5]Metabolomics, Proteomics and Mass Spectrometry Cores, University of Utah, Salt Lake City, UT, 84112
[6] Department of Nutrition and Integrative Physiology and the Diabetes and Metabolism Research Center, University of Utah, Salt Lake City, UT 84112

Short title: Schistosomes reprogram myeloid metabolism

Corresponding Author:

Keke Fairfax
Department of Pathology
Division of Microbiology and Immunology
University of Utah
JMRB 2200B
15 N Medical Drive East
Salt Lake City, UT 84112
Email: keke.fairfax@path.utah.edu
ORCID: https://orcid.org/0000-0002-8382-2960
801-581-5980 (office)

Abstract

Despite strong evidence that helminth infections are protective against the development of metabolic disease, a major gap exists in understanding the mechanism(s) underlying this. We have previously found that *Schistosoma mansoni* induces profound alterations to the metabolic transcriptome of hepatic macrophages and protects male ApoE$^{-/-}$ on high fat diet from the development of obesity, glucose intolerance, and atherosclerosis. Here we demonstrate that macrophages derived from the bone marrow (BMDM) of *S. mansoni* infected male ApoE$^{-/-}$ mice have dramatically increased mitochondrial respiration and mitochondrial mass compared to those from uninfected mice. This change is accompanied by increased glucose and palmitate shuttling into TCA cycle intermediates and decreased accumulation of cellular cholesterol esters. The systemic effects of metabolic modulation by schistosome infection are a function of biological sex, where schistosome infection protects ApoE$^{-/-}$ male mice from obesity, glucose intolerance, and increased serum triglycerides, but not female mice. The sex-dependent effects of infection extend to myeloid cells specifically, where metabolic reprogramming leads to opposite cholesterol phenotypes in BMDM from infected females and males. Finally, we demonstrate that the metabolic reprogramming of male myeloid cells is transferrable via bone marrow transplantation to an uninfected host, indicating maintenance of reprogramming in the absence of ongoing schistosome antigen exposure. This work provides strong evidence that *S. mansoni* systemically reprograms the metabolism of the myeloid compartment in a sex-dependent manner.

Author Summary

Globally helminth endemic regions have lower incidences of metabolic disease. Schistosomiasis in particular has been shown to protect male mice from the development of atherosclerosis, diabetes and obesity while altering the metabolism of liver macrophages. In this present study we sought to understand if metabolic modulation occurs systemically, and if these effects occur in females as well. We have found for the first time that macrophages generated from bone marrow myeloid progenitors from infected male mice have long-lived increases in their basal metabolism of lipids. We have also found that unlike male mice, female mice infected with *Schistosoma mansoni* are not protected from the development of diabetes and obesity. *S. mansoni* infection induces opposite changes to macrophage transcription and metabolism in males and females. Importantly we demonstrate that the changes to male macrophage metabolism can be transferred to an uninfected host. This suggests that metabolic reprogramming is long-lived without exposure to active infection, and the development of a memory-like phenotype.

Introduction

Cardiovascular disease (CVD) is the leading worldwide cause of mortality [1, 2]. In the United States, 65% of adults diagnosed with diabetes have elevated LDL cholesterol levels or take cholesterol lowering medications, and death rates from atherosclerotic cardiovascular disease (CVD) are ~1.7 times higher in this population as compared to non-diabetic adults [3]. It is well established that in the diabetic population, obesity, and dyslipidemia are risk factors underlying these increases in mortality, while hyperglycemia is an independent risk factor [4, 5]. Underlying conditions such as diabetes and atherosclerosis contribute to the burden of CVD in both females

90 and males. While, the incidence of CVD is markedly higher in men than in age-matched women
91 [6, 7], the risk of developing CVD while diabetic is much greater in women than men [8, 9]. In
92 non-diabetic patients, females exhibit increased insulin sensitivity in comparison to males, as
93 well as reduced prevalence of dysglycemia and enhanced muscle glucose uptake [10-13],
94 suggesting sex-dependent modulations in whole body metabolism. Recent studies suggest a role
95 of the gut microbiota in the differences between sexes in the regulation of lipid metabolism [14].
96 Nevertheless, complete understanding of mechanistic basis behind sexual dimorphism in
97 metabolic syndrome is still lacking.
98
99 Previous studies have uncovered an association between a history of helminth infection and
100 reduced prevalence of metabolic disease in humans and rodents ([15-17]. Specifically, infection
101 by Schistosomes reduces cholesterol and atherosclerotic plaques [15, 16], this effect has been
102 attributed, in part, to an anti-inflammatory phenotype in macrophages [18] and transcriptional
103 reprogramming of phospholipid and glucose metabolism related genes in hepatic macrophages
104 [19]. Moreover, it has been postulated that schistosomes have the potential to affect long term
105 glucose metabolism in T cells [20]. Accumulating evidence suggests that biological sex affects
106 disease progression; yet the effect of schistosomiasis on metabolic-protection in females and
107 males it is not well understood, as most studies have been conducted only in males or no sex
108 differentiation has been made during data analysis ([21-23]). To date, no report with a particular
109 emphasis on females has been conducted.
110
111 Schistosomiasis induces Th2 polarization and alternative activation of macrophages, essential for
112 host survival [24-26]. IL-4 induced alternative activation of macrophages relies on oxidative

113 phosphorylation (OXPHOS) and fatty acid oxidation for energy production, and is dependent on
114 cell intrinsic lysosomal lipolysis [27, 28]. Macrophage metabolism follows a dysmorphic pattern,
115 as sex-related differences affect the processes involved in cholesterol and lipid metabolism in
116 macrophages as well as inflammatory cytokine production in adipose tissue [29, 30]. Moreover,
117 in rats, phagocytes from females had increased ROS generation than males [31]. Such
118 differences have often been attributed to the role of sex hormones in gene expression and
119 immune cell function [32-34], but a clear understanding of the effects of sex on the regulation of
120 macrophage metabolism, as well as how sex modulates the effects of schistosomiasis in the
121 protection from metabolic disease is lacking.
122
123 In the present study, we sought to determine the systemic effects of *S. mansoni* infection on the
124 myeloid lineage. Surprisingly, we discovered that macrophages derived from the bone marrow of
125 *S. mansoni* infected male mice have dramatically increased oxygen consumption and
126 mitochondrial mass compared to those from uninfected males. This shift is accompanied by
127 increased carbon shuttling into TCA cycle intermediates, a decrease in cholesterol esters, and
128 increased fatty acid oxidation. When we examined the role of biological sex in schistosome
129 induced modulation we found that *S. mansoni* infection does not reliably protect ApoE$^{-/-}$ female
130 mice from HFD induced weight gain or glucose intolerance. The sex-dependent effect of
131 infection extends to the myeloid lineage, where bone marrow derived macrophages from infected
132 females display the opposite metabolic phenotype as those from infected males, with a dramatic
133 increase in cellular cholesterol esters. Overall, these data present the first evidence that *S.*
134 *mansoni* systemically modulates the myeloid compartment in a sex-dependent manner and

135 provide a more comprehensive understanding of how *S. mansoni* infection may confer metabolic
136 protection at the cellular level.
137
138 **Results**
139 **Macrophages derived from *S. mansoni* infected male mice have increased oxygen**
140 **consumption and spare respiratory capacity**
141
142 We have previously reported that schistosomiasis alters the expression of numerous genes
143 relevant to glucose, cholesterol, and amino acid metabolism in hepatic macrophages of male
144 mice [19]. These alterations are associated with improved insulin sensitivity and atherosclerotic
145 score in male mice. Since it has previously been shown that during *S. mansoni* infection the
146 majority of liver macrophages are monocyte derived, and monocyte recruitment drives both
147 atherosclerosis [35, 36] and obesity induced insulin resistance [37-40], we hypothesized that
148 Schistosome infection may imprint the monocyte- macrophage lineage with altered metabolic
149 propensities. To elucidate whether infection imprints macrophages with an altered metabolic
150 phenotype we infected (and mock infected controls) atherogenesis-prone male $ApoE^{-/-}$mice on
151 high-fat diet (HFD), and sacrificed them at 10-weeks post-infection to harvest bone marrow
152 cells. Macrophages were differentiated *in vitro* with M-CSF in a 6-7-day culture. We performed
153 real-time extracellular flux analysis on unstimulated bone marrow derived macrophages
154 (BMDM) from $ApoE^{-/-}$ HFD infected and uninfected (control) HFD mice to quantify oxygen
155 consumption rate (OCR) (Figure 1A). BMDM from $ApoE^{-/-}$ HFD infected mice showed
156 improved basal respiration (Figure 1B) and significantly increased spare respiratory capacity
157 ($p<0.0001$, Figure 1C). Since eukaryotic cells integrate oxidative phosphorylation (OXPHOS),

158 glycolysis and the tricarboxylic acid (TCA) cycle to satisfy energy requirements, we also tested
159 the extracellular acidification rate (ECAR), which is suggested as a marker of inhibited
160 mitochondrial respiration [41], in BMDM from infected and uninfected ApoE$^{-/-}$ HFD mice. We
161 observed no differences in ECAR in infected male mice compared to uninfected controls (Figure
162 1D). Cell intrinsic lysosomal lipolysis has previously been shown to support macrophage spare
163 respiratory capacity in the context of macrophage alternative activation [28, 42]. We stained for
164 hydrophobic and neutral lipids by Oil Red O (ORO) [43] and observed that the lipid content of
165 BMDM from infected ApoE$^{-/-}$ males trended to reduction in comparison to the control group, but
166 was not significantly reduced (Figure 1E). To analyze BMDM mitochondrial mass, which has
167 also been linked to increased respiratory capacity [44], we analyzed mitochondrial activity by
168 Mitotracker Deep Red FM. We observed that BMDM from infected mice exhibited increased
169 MitoTracker median fluorescent intensity (MFI) in comparison to the BMDM from uninfected
170 mice (Figure 1F). Overall, these data indicate that *S. mansoni* infection in males leads to
171 increased oxygen consumption and mitochondrial metabolism in BMDM. Mitochondrial
172 oxidative dysfunction in macrophages has recently been linked to insulin resistance [45], so this
173 metabolic shift could contribute to the infection-induced improvement in glucose tolerance seen
174 in infected males .
175
176 **Schistosomiasis in male ApoE$^{-/-}$ mice alters metabolic flux of glucose and the lipidomic**
177 **fingerprint of macrophages**
178
179 In order to understand how Schistosome infection alters the metabolic fingerprint and promotes
180 mitochondrial metabolism in macrophages derived from ApoE$^{-/-}$ HFD male mice, we performed

181 metabolic tracing analysis, where macrophages were differentiated in the presence of normal
182 glucose and then switched to ^{13}C-labeled glucose for 24 hours. We observed increased shuttling
183 of heavy labeled glucose to malate (Figure 2A), citrate (Figure 2B), itaconate (Figure 2C), and
184 succinate Figure 2E in BMDM from infected mice in comparison to BMDM from uninfected
185 mice. The lack of increased heavy lactate production (Figure 2D), suggests that the primary
186 reprogramming is focused on glucose-dependent mitochondrial metabolism. Importantly, we
187 found no upregulation of alternative activation markers (CD301, CD206, Arg1, Nos2) in
188 unstimulated BMDM from infected mice when compared to BMDM from controls
189 (Supplementary Figure 1). Since we have previously shown that infection alters the phospholipid
190 and cholesterol metabolism in hepatic macrophages [46], we performed unbiased lipidomics
191 using liquid chromatography-mass spectrometry (LC-MS). We used a supervised model by
192 partial least squares-discriminant analysis (PLS-DA), with two components to determine the
193 lipidomic profile of BMDM. There was a robust separation between groups that indicates the
194 metabolic profiles of BMDM from infected and uninfected males differ significantly and
195 suggests that there is a prominent alteration of metabolites induced by infection in male mice
196 (Figure 2F). The lipid species that drive the variation observed in the PLS-DA as measured by
197 the Variable Importance in Projection (VIP) score from uninfected males in comparison to
198 infected males included cholesterol esters (CE) (20:1), CE (22:0), CE (24:0), CE (24:1), CE
199 (22:4), CE (22:1), CE (18:0); diacylglycerols (DG) (16:0_16:0), DG (16:0_18:0) and
200 triacyclglycerol (TG) (16:0_16:0_16:0) (Figure 2G,H). We then analyzed the total CE levels in
201 macrophages from both groups of male mice and found that infection led to significantly reduced
202 CE in male mice ($p<0.0001$, Figure 2I), further evidencing an important role of cholesterol
203 metabolism in macrophages following helminth infection. Next, we determined the

204 transcriptomic modifications induced by infection in unstimulated BMDM from infected and
205 uninfected males by mRNA sequencing (mRNAseq). Significant gene expression differences
206 were observed in BMDM from infected male mice, compared to uninfected controls. Transcripts
207 from the two groups are depicted in Volcano plots, using false discovery rate (FDR<0.05 in red,
208 FDR<0.01 in blue) and Log2 fold changes (cut off of .6 Log2 FC) to identify statistically
209 significant genes (Figure 2J). Among the differentially regulated factors are Gbp6, which is
210 related to interferon-γ signaling and innate immune function; Gm7609, a predicted pseudogene;
211 Gbp4, a member of the GTPase family involved in protective immunity against microbial and
212 viral pathogens; Apol9a, which is predicted to be related to lipid transport, lipoprotein metabolic
213 processes and stimulated by interferon; Iigp1, a GTPase with roles in response to intracellular
214 pathogens; CD300e, which belongs to families of paired activating and inhibitory receptors
215 implicated in immune responses; and Batf2, a basic leucine zipper factor whose activation is
216 detrimental for type-1 infectious disease. Importantly, Mgll, which encodes monoacylglycerol
217 lipase that catalyzes the conversion of monoacylglycerides to free fatty acids and glycerol was
218 significantly increased. Mgll is required for lipolysis and improved glucose homeostasis in mice
219 on HFD [47, 48], an infection driven increase was validated by RT-qPCR (Figure 2L). In
220 addition, Slc1a3, which encodes for the glutamate aspartate transporter 1 that is localized in the
221 inner mitochondria membrane as part of the malate-aspartate shuttle and is relevant for amino
222 acid homeostasis in adipocytes, was significantly altered in our model, and was further validated
223 by RT-qPCR (Figure 2M). Interestingly, the pathways significantly altered (Figure 2K) during
224 infection included hematopoietic cell lineage ($p=5.779 \times 10^{-8}$), asthma ($p=3.169 \times 10^{-5}$), and
225 cytokine-cytokine receptor interactions, graft-versus host disease, type 1 diabetes and allograft
226 regression (p=0.0000894). Together, these data identify key factors in immune and metabolic

227 responses as well as novel factors with unknown functions that are regulated by exposure to *S.*
228 *mansoni* infection.
229
230 **_S. mansoni_ infection protects male mice, but not female mice, from obesity and glucose**
231 **intolerance independently of systemic alternative macrophage activation**
232
233 Sex is a key contributor to the phenotype of cardiovascular and metabolic features in mammals
234 [49], so we assessed the sex dependent impact of *S. mansoni* infection on obesity and glucose
235 intolerance. For this, we fed male and female ApoE$^{-/-}$ HFD for 10-days before infection. We
236 infected and mock infected mice (controls) as described in the methods. Ten weeks post
237 infection we analyzed body weight and glucose tolerance (via an IP glucose tolerance test) and
238 found that infection is significantly beneficial for male, but not female mice, as only males are
239 protected from HFD-induced weight gain and glucose intolerance (Figure 3A, 3B). We also
240 analyzed serum triglyceride (TG) and diglyceride (DG) levels using untargeted lipidomics and
241 found that relative abundance of both TG and DG were decreased in infected males as compared
242 to uninfected males, while TGs were increased by infection in females and DGs were unchanged
243 (Figure 3C). These data indicate that *S. mansoni* infection induces a sex-dependent modulation
244 of metabolic disease parameters. We then wondered if this infection-mediated effect in males
245 only was correlated with differences in systemic alternative activation of hepatic macrophages in
246 females. Flow cytometry analysis showed that alternative activation markers (CD206, CD301,
247 Arg1) were highly expressed in macrophages from male and female mice following infection,
248 but not in naïve mice (Figure 3D), suggesting that *S. mansoni* induced alternative activation
249 irrespective of sex. Previous studies characterizing the dynamics of alternatively activated

250 macrophages during schistosome infection have found that these macrophages primarily arise
251 from Ly6C^{high} monocytes [50, 51]. Naïve male and female ApoE$^{-/-}$ mice on HFD had equivalent
252 frequencies of Ly6c^{high} monocytes circulating in peripheral blood. At 10-weeks post infection we
253 found an increased percentage of both Ly6C^{int} and Ly6C^{high} cells (Figure 3E) in both male and
254 female mice compared to the mock infected controls, with the frequency of Ly6C^{high} cells in
255 females 1.74 times that of males, suggesting either increased monopoiesis in females, or
256 increased tissue recruitment in males . Since we had found increased mitochondrial MFI in
257 BMDM from infected male mice, we asked whether circulating blood monocytes are similarly
258 modulated. We observed an infection induced increase in Mitotracker fluorescent intensity in
259 monocytes from male ApoE$^{-/-}$ mice on HFD, but not from females (Figure 3F). These data
260 suggest that there is sex-specific increased mitochondrial activity following infection in the
261 monocyte cell population. We then wondered if these effects in the differentiated monocytes are
262 the result of long-lasting changes in the myeloid lineage after helminth infection. For this, we
263 analyzed the main lineages of hematopoietic progenitors that produce myeloid cells:
264 granulocyte-monocyte progenitors (GMP), monocyte-DC progenitors (MDP) and the common
265 myeloid progenitor (CMP) in female and male ApoE$^{-/-}$ mice. CMP were defined as Lin^{-}CD127^{-}c-
266 Kit^{+}Sca-1^{-}CD34^{+}FcRII/III$^{lo/-}$[52], GMP were defined as Lin^{-}IL-7R^{-}Sca-1^{-}c-kit^{+}CD34^{+}FcR
267 II/III^{+}, and MDP were defined as defined as Lin^{-} c-Kit^{+} Sca-1^{-} CD34^{+} FcγR^{lo} CD115^{hi} cells.
268 Overall bone marrow cellularity was not affected by Schistosome infection (Figure 3G),
269 however, the numbers of CMP and GMP in infected male mice were significantly reduced
270 compared to uninfected controls, while GMP and CMP were not reduced in females (Figure 3 H-
271 J). The numbers and percentages of MDP remained unchanged in infected females and males
272 compared to uninfected controls (Figure 3K, 3L). These data suggest that *S. mansoni* infection

273 modulates both metabolic disease and the myeloid lineage in a sex-specific manner that is
274 independent from the induction of systemic alternative activation.
275
276 ***S. mansoni*-increases fatty acid oxidation in male but not female ApoE$^{-/-}$ mice on HFD**
277
278 In order to determine whether infection-induced pathologic differences in males and females
279 were accompanied by sex-specific differential macrophage metabolic regulation, we cultured
280 bone marrow cells from 10-week infected or uninfected control male and female mice for 7 days
281 to generate BMDM. OCR was measured in real time in basal conditions and following the
282 addition of mitochondrial inhibitors in unstimulated BMDM from both infected and uninfected
283 male and female ApoE$^{-/-}$ animals. Similar to as seen in Figure 1A, BMDM from infected males
284 exhibited increased basal OCR and spare respiratory capacity compared to uninfected male
285 controls (Figure 4A, 4B, 4C). However, basal OCR and spare respiratory capacity of BMDM
286 from infected females remained unaltered in comparison to BMDM from uninfected females
287 (Figure 4A, 4B, 4C). Moreover, side by side OCR analysis in females and males with palmitate
288 as a substrate (glucose limiting conditions) showed that BMDM from infected male, but not from
289 infected females had an increased ability to oxidize exogenous palmitate (Figure 4D). In
290 addition, BMDM from infected males but not females had significantly increased palmitate basal
291 OCR and palmitate spare respiratory capacity, suggesting exogenous free fatty usage as a carbon
292 source for OXPHOS (Figure 4E, 4F). Similar to the male only data, we observed no differences
293 in macrophage lipid content in either group, suggesting that global lipolysis may not underlie
294 OCR and spare respiratory capacity in our model (Figure 4G). Additionally, analysis of
295 mitochondrial mass in females and males showed that similar to blood monocytes, BMDM from

296 infected male mice, but not females have a significantly higher Mitotracker MFI. These data
297 suggest that *S. mansoni* infection improved mitochondrial biogenesis in males, but not females.
298 Again, suggesting differential regulation of macrophage metabolism based on biological sex.
299 This regulation may account in part for the differences in the role of infection in modulating
300 obesity and insulin sensitivity.
301
302 ***S. mansoni* infection differentially alters the cellular lipid profile in female and male mice**
303
304 To understand the sex specific modulations induced by schistosomiasis in macrophage lipid
305 metabolism, we isolated cellular lipids from unstimulated BMDM and performed unbiased
306 lipidomics in male and female derived-cells. PLS-DA showed that *S. mansoni* infection led to a
307 sex-specific lipid profile (Figure 5A). Further, analysis of total CE (identified as a VIP species in
308 males in Figure 2) showed that infection led to decreased levels of CE in cells derived from
309 infected male mice. In contrast, infection led to significantly increased total CE in BMDM
310 derived from infected female mice (Figure 5B). Similar to males, infection in females induces a
311 unique lipid signature (Figure 5C), with two species of plasmanyl-PE, three species of
312 plasmanyl-PC, BMP and CE as the main drivers of the altered lipid profile in females during
313 infection (Figure 5D). Since we observed BMP's as a VIP compound driven by *S. mansoni*
314 infection in females, but not males, we went back and performed targeted lipidomics to quantify
315 BMPs at the class level. Indeed, total BMPs were significantly increased by infection in BMDM
316 from females but not males (Figure 5E). Our Seahorse data indicates that *S. mansoni* infection
317 induced differential oxidation of exogenous palmitate in BMDM derived from males and
318 females. In order to understand the metabolic flux of exogenous palmitate, we performed

319 metabolic tracing analysis of palmitate, where macrophages were differentiated in the presence
320 of normal glucose and then switched to C^{13}-labeled palmitate for 24 hours. Similar to what we
321 documented with glucose, we observed increased shuttling of heavy labeled palmitate into
322 succinate, malate, and fumarate in BMDM derived from infected males, with decreased shuttling
323 into myristate (a marker of fatty acid elongation). BMDM derived from infected females
324 displayed the opposite phenotype, with decreased shuttling of heavy labeled palmitate into
325 succinate, malate, and fumarate, and increased shuttling into myristate compared to BMDM from
326 uninfected controls. These data suggest that BMDM derived from infected male $ApoE^{-/-}$ mice
327 have increased basal utilization of exogenous palmitate for beta-oxidation, while the female data
328 suggests increased lipid synthesis, strengthening the data obtained from our palmitate
329 extracellular flux analysis.
330 To further understand the role of biological sex in the *S. mansoni* induced reprograming of the
331 BMDM lipidome, we isolated cellular lipids from male and female BMDM either unstimulated
332 (media), or following LPS stimulation, and then performed untargeted lipidomics as described in
333 Figure 5. We analyzed the lipidomic data with machine learning using a two-step selection
334 process (see Methods). This approach identified ~20 features (lipid compounds) contributing to
335 an elastic net regression model that can predict the infection status of samples-originating
336 animals [53]. These informative features are listed in descending order of importance
337 (Supplemental Figure 2A). Interestingly, some key features (for instance, the top scoring one) are
338 not represented as significant in the univariate tests (univariate adjusted p values, Supplemental
339 Figure 2B). However, these features are important contributors to the multivariate machine
340 learning model. This is not unexpected – some features that would be considered uninformative
341 individually may be very useful in improving predictions if combined with other features. When

342 we examine these features individually, we can see a differential response to infection for males
343 and females (for instance, PG 18:1_18:2, a glycerophospholipid) represented in Supplemental
344 Figure 2C). Seven of the 20 molecular features identified by machine learning are BMP
345 (Bis(monoacylglycerol)phosphate) species, which have been implicated in glycosphingolipid
346 degradation and cholesterol transport [54, 55]. These data further support the hypothesis that *S.*
347 *mansoni* infection differentially modulates the metabolism of myeloid cells from male and
348 female animals, and that this modulation revolves around decreased cholesterol storage and fatty
349 acid synthesis in males and increased cholesterol storage and fatty acid synthesis in females.
350 Cholesterol and lipid metabolism has previously been associated with inflammatory myeloid
351 effector function [56-58], so we quantified the acute inflammatory effectors nitrite and iNOS,
352 along with pro-inflammatory cytokines/chemokines IL-12p70, CXCL1, and IL-6
353 (chemokines/cytokines with known pathogenic roles in obesity, insulin resistance and
354 atherosclerosis) following stimulation with LPS. *S. mansoni* infection increases LPS induced
355 nitrite and iNOS production in BMDM from male, but not female ApoE$^{-/-}$ mice on HFD (Figure
356 5 J,K). Conversely, BMDM from infected males have decreased production of IL-2p70, CXCL1,
357 and IL-6 (Figure 5 L-N) following LPS stimulation as compared to BMDM from uninfected
358 controls. LPS induced IL-12p70, CXCL1, and IL-6 production by female BMDM is unaffected
359 by infection status. Increased production of the effector molecules nitrite and iNOS combined
360 with decreased production of pro-inflammatory mediators associated with chronic inflammation
361 supports the idea that *S. mansoni* infection promotes a hybrid macrophage state in males.
362
363 ***S. mansoni* infection modulates the myeloid transcriptome in a sex-specific manner**

364 Since we documented significant sex dependent shifts in functional metabolism in BMDM from
365 male and female *S. mansoni* infected mice, we sought to determine if differential transcriptional
366 modulation underlies these shifts. In order to investigate the genes and respective pathways that
367 were associated with specific conditions and the ones that were differentially regulated by sex we
368 performed mRNAseq on unstimulated BMDM derived from male and female ApoE$^{-/-}$ mice at 10-
369 weeks post *S. mansoni* or mock infection. We identified different subsets of genes that were
370 preferentially upregulated in males ($p<0.05$, Figure 6A). Among 1448 genes upregulated in
371 males regardless of infection status with a p value <0.05, the majority of these (238 genes) were
372 associated to metabolic functions by pathway analysis. Of these 238 genes involved in
373 metabolism we identified hexokinase 1 (hk1), citrate synthase (cs), apolipoprotein A2 (apoa2),
374 aldehyde dehydrogenase 3 family member A2 (aldh3a2), lipoyltransferase (lipt1), solute carrier
375 family 19 member 1 (slc19a1), LDL receptor related protein 1 (lrp1), many of these are involved
376 in lipoprotein and cholesterol metabolism. These data suggest that myeloid metabolism is
377 differentially regulated by sex, at least in the context of HFD. In addition, we found 216 genes
378 involved in immunity. Among these genes with immune function we identified interleukin 10 (il-
379 10), Toll like receptor 5 (tlr5), NLR family pyrin domain containing 3 (nlrp3), inducible T cell
380 costimulatory (icos), which have diverse pro and anti-inflammatory function in the immune
381 system. Next, we surveyed the genes that are differentially regulated in males and females
382 following *S. mansoni* infection. We found 66 genes involved in metabolism, hemostasis, the
383 adaptive immune system, collagen degradation and not annotated to specific pathways.
384 Following the genes with known function, the majority (10) of differentially regulated genes
385 have documented roles in metabolism. Among these, we identified type II iodothyronine
386 deiodinase (dio2), which has been implicated in the regulation of diet induced obesity [59, 60].

387 Moreover, we found that hexokinase 3 (hk3), fatty acid binding protein 4 (fabp4), sphingomyelin
388 synthase 2 (sgms2), solute carrier family 6 member 8 (slc6a8) were all upregulated in male and
389 downregulated in female BMDM following *S. mansoni* infection (Figure 6B). In addition, we
390 performed gene ontology analysis from the 66 genes that were differentially regulated in females
391 and males. The most significant pathways were response to glucocorticoids, glycoprotein
392 metabolism, and fatty acid metabolism, again suggesting that there is a sex-specific metabolic
393 response to *S. mansoni* infection in myeloid cells. These pathways may help explain the
394 differential metabolic modulation induced by schistosomiasis in males and females (Figure 6C).
395

396 ***S. mansoni* induced modulation of male macrophage metabolism is long-lived in the**
397 **absence of antigen**

398 Our metabolic and transcriptomic data from BMDM differentiated *in vitro* from male *S. mansoni*
399 infected mice suggested that metabolic modulation may be long-lived in the absence of ongoing
400 antigen exposure. In order to determine durable nature of modulation we transferred bone
401 marrow from either 10-week *S. mansoni* infected male ApoE$^{-/-}$ mice on HFD, or uninfected male
402 controls into busulfan treated recipient ApoE$^{-/-}$ mice on HFD. At 10 weeks post-bone marrow
403 transfer we assayed glucose tolerance via an i.p. GTT. Mice that received bone marrow from
404 infected males have a significantly lower glucose area under the curve (AUC) than those that
405 received control bone marrow. We harvested bone marrow from all recipients and differentiated
406 BMDM in M-CSF for 6 days and then performed real-time extracellular flux analysis. BMDM
407 from recipients of bone marrow from *S. mansoni* infected mice had significantly higher basal
408 oxygen consumption and a trend towards increased spare respiratory capacity as compared to
409 BMDM generated from recipients of uninfected control bone marrow. Additionally, BMDM

410 from recipients of bone marrow from *S. mansoni* infected mice had a significantly higher
411 Mitotracker MFI than BMDM from recipients of control bone marrow. These data suggest that *S.*
412 *mansoni* induced metabolic modulation of the myeloid lineage in males is long-lived even in the
413 absence of ongoing exposure to egg antigens, and that hematopoietic cells are at least partially
414 responsible for the regulation of whole-body glucose metabolism in the HFD ApoE$^{-/-}$ model.

415 **Discussion**

416 Helminth infections in general, and schistosomiasis in specific, have been known to be
417 inversely correlated with obesity and glucose intolerance for over a decade, a phenomenon
418 thought to be associated with Type 2 polarization of macrophages and T cells. In the current
419 study we report that *S. mansoni* infection induces dramatic metabolic alterations in BMDM from
420 male ApoE$^{-/-}$ mice on HFD. Our results indicate that macrophages derived from the bone marrow
421 of infected male mice have increased basal oxygen consumption and spare respiratory capacity
422 compared to those derived from uninfected males. In T cells, an increase in spare respiratory
423 capacity has been linked to mitochondrial biogenesis, and controls the transition to a long-lived
424 memory phenotype [61]. In macrophages, M2 (alternative) activation has previously been shown
425 to lead to increased spare respiratory capacity, a process that also involves mitochondrial
426 biogenesis [62], while TLR recognition of bacteria has been shown to increase mitochondrial
427 respiration via modulation of complex I and II [63] . In both cell types, the increased
428 mitochondrial respiration underlies the longevity of the cells. In our model we have not found
429 most of the traditional markers used to define M2 alternative activation by flow cytometry at
430 steady state (Supplemental Figure 1). Arg1 is the only canonical M2 transcript that is modulated
431 in the BMDM from infected male mice at steady state, and that fold increase is relatively low
432 (.894 log FC, adjusted *p*-value =.035). Arg1 drives the production of polyamines, which in turn

433 are able to modulate mitochondrial OxPHOS [64, 65]. In the currently accepted paradigm of M2
434 polarization stat6 phosphorylation upregulates PGC1-β and PPARγ, leading to mitochondrial
435 biogenesis and increased beta-oxidation in addition to Arg1transcription. Here we present a
436 model where neither PGC1-β or PPARγ are modulated, but Arg1 transcription is increased with
437 a concomitant dramatic increase in mitochondrial respiration, suggesting that there may be
438 alternative ways to modulate mitochondrial metabolism.

439 Alternative activation has previously been shown to be dependent on cell intrinsic
440 lysosomal lipolysis and lal, with the defining feature being reductions in lipid droplets [28]. In
441 our model using unstimulated BMDM from *S. mansoni* infected mice there is no gross difference
442 in lipid droplets, nor an increase in lal transcripts. Instead, we found a significant shift in the
443 lipidome of BMDM from infected male mice that centered on a reduction in cholesterol esters.
444 Previously published work in IL-4 induced M2 macrophages has found that lipolysis centered on
445 TGs as a fatty acid source. While we did find reductions in two species of DGs and one species
446 of monoacylglycerol (MG), there were no significant alterations to TAGs in the BMDM
447 generated from infected males. Flux analysis with heavy carbon labeled glucose and palmitate
448 suggest that BMDM from male infected mice have increased shuttling of both glucose and
449 palmitate into TCA cycle intermediates, suggesting that these cells have increased mitochondrial
450 beta oxidation. In addition to the unique lipidomic modulations, we found that the dramatic
451 increase in both basal oxygen consumption and spare respiratory capacity we observed in
452 BMDM from male infected mice was significantly palmitate dependent. This observation further
453 supports the idea that *in vivo* exposure of myeloid precursors to helminth antigens induces
454 unique metabolic modulations that focus on cholesterol and lipid metabolism as a source for
455 palmitate for beta oxidation. These data suggest that hybrid metabolic states in the absence of

456 M1 or M2 polarization occur in macrophages in the context of chronic disease, and present a
457 challenge to the dichotomy of M1 versus M2 activation being driven by immunometabolism.
458 Future studies exploring the immunometabolism of bone marrow derived and tissue resident
459 macrophages and dendritic cells from other chronic infections and inflammatory diseases are
460 needed in order to obtain a true picture of the correlation between metabolism and myeloid
461 polarization.

462 There are significant clinical differences in both the etiology and pathology of diabetes
463 and cardiovascular disease between males and females, but sex differences in immunological
464 activation or modulation by *S. mansoni* infection have not previously been studied in humans or
465 animal models. Surprisingly, we found that the unique metabolic modulations induced by *S.*
466 *mansoni* infection in BMDM from male mice do not occur in females, and infected females are
467 not reliably protected from high-fat diet induced obesity or glucose intolerance. Interestingly,
468 hepatic macrophage alternative activation in response to infection is equivalent between males
469 and females, but infection increases blood monocyte frequency in females to a much greater
470 extent than in males, suggesting sex specific modulation of either monopoiesis or monocyte
471 recruitment into tissues. Blood monocytes from infected males phenocopy the increase in
472 Mitotracker MFI that we have found in BMDM generated from infected males, indicating that
473 our BMDM model is likely an accurate representation of the *in vivo* potential of the myeloid
474 compartment. Interestingly, we found that infection significantly reduced the total number of
475 CMP and GMP in male, but not female bone marrow, again pointing to a sex-specific
476 modulation of the myeloid lineage at the precursor level. The reduction of CMP and GMP in
477 infected males suggests either an increase in the rate of differentiation into
478 monocytes/granulocytes, or decreased homeostatic proliferation. Since males have fewer blood

479 monocytes than female, we favor the later possibility. These possibilities and the relationship
480 between reductions in numbers of CMP and GMP in males, and the functional metabolic
481 differences in BMDM will be explored in future work.
482
483 Analysis of the BMDM transcriptomes from males and females revealed that over a
484 thousand genes are up regulated in male versus female BMDM regardless of *S. mansoni*
485 infection state. At the same time, over five dozen are differentially regulated by infection.
486 Focusing on the genes that are up-regulated in BMDM from infected males and down-regulated
487 in females, we found more than ten genes with known functions in cellular metabolism. Some of
488 these genes, like PFKFB3, have known regulatory elements for progesterone and estrogen [66],
489 but some of them, like fabp4, have no published mechanism of sex hormone regulation.
490 Glycolysis and cholesterol metabolism have previously been shown to directly affect the
491 inflammatory potential of myeloid cells. Our data indicate that *S. mansoni* infection induces a
492 hybrid inflammatory state in male but not female BMDM, where the LPS induced production of
493 nitrite and iNOS is enhanced, while the production of the key chronic pro-inflammatory
494 mediators IL-12p70, CXCL1, and IL-6 are reduced. This inflammatory profile is distinct from
495 what has previously been published with IL-4 induced M2 macrophages, where the production of
496 iNOS and nitrite are reduced following TLR stimulation [67]. CXCL1 and IL-6 have previously
497 been linked to increased monocyte recruitment and disease progression in both atherosclerosis
498 and obesity-induced diabetes [68-72], so these data support the possibility of infection driven
499 modulation of macrophage function supporting the decreased pathology seen in infected males.
500 We have demonstrated that the modulation of macrophage oxygen consumption is transferrable
501 to an uninfected recipient, and can last for at least ten weeks, suggesting that in males, *S.*

502 *mansoni* infection induces long-lived metabolic modulation of the myeloid lineage that survives
503 in the absence of ongoing antigenic exposure. Trained innate immunity has previously been
504 documented to be induced by BCG immunization [73], and has recently been suggested to be the
505 mechanism underlying the association between previous bacterial and fungal infections and the
506 development of atherosclerosis [74, 75]. In these models, trained immunity and epigenetic
507 reprogramming is driven in part from a switch from oxidative phosphorylation to increased
508 aerobic glycolysis [76, 77]. In the case of BCG, trained circulating monocytes can be found
509 months after immunization, which strongly suggests reprogramming of bone marrow progenitors
510 [78]. Recent reports indicate that western high-fat diet itself also induces innate training of bone
511 marrow progenitors in both the $Ldr^{-/-}$ model of atherosclerosis [79] and in obesity related
512 steatohepatitis [80]. Our data suggests that *S. mansoni* infection in males trains the myeloid
513 lineage in the opposite fashion; modulating the metabolic transcriptome of the myeloid lineage
514 such that oxidative phosphorylation and mitochondrial activity is increased, while the chronic
515 inflammatory potential is decreased. Alterations to the numbers and frequency of myeloid
516 progenitors and the transferability of our phenotype via bone marrow suggests that progenitors
517 are indeed modulated in our model, the relative role of epigenetic modulation versus microRNA
518 regulation in dictating the *S. mansoni* induced myeloid transcriptome will be the subject of future
519 studies.

520 There are significant differences in both the susceptibility and disease presentation
521 between males and females for both diabetes and cardiovascular disease, but few studies have
522 focused on the role of immunometabolism in this dichotomy. Our data suggests apparent
523 biological sex-dependent differences in both the ability of schistosomes to protect from the
524 development of HFD induced metabolic disease parameters, and the ability to modulate

525 macrophage glucose and lipid metabolism. The current epidemiological data strongly indicates
526 an inverse correlation between helminth infections and metabolic diseases such as diabetes and
527 cardiovascular disease, but these studies were not designed to identify sex-specific correlations.
528 Few animal studies have focused on the role of myeloid cells in driving sex-specific metabolic
529 differences. Our current data indicate a clear need for further studies in both humans and animal
530 models to specifically probe the relationship between biological sex and myeloid metabolism,
531 and how chronic helminth infections modulate this.
532

533 **Conflict of Interest**

534 The authors declare no competing interests.
535

536 **Materials AND Methods**

537 **Parasite and Mouse Models**

538 This study was carried out in accordance with the recommendations in the Guide for the Care
539 and Use of Laboratory Animals of the National Institutes of Health. The protocols were
540 approved by the Institutional Animal Care and Use Committees of the University of Utah. Snails
541 infected with *S. mansoni* (strain NMRI, NR-21962) were provided by the Schistosome Research
542 Reagent Resource Center for distribution by BEI Resources, NIAID NIH. Male and female
543 ApoE$^{-/-}$ (B6.129P2-Apoetm1Unc/J) were purchased from the Jackson Laboratories and bred at
544 the University of Utah. Mice were housed in pathogen-free conditions and were fed standard
545 rodent chow (2019 rodent chow, Harlan Teklad) until 10-14 days before infection when they
546 were transitioned to a high-fat diet (HFD: 21% milk fat, 0.15% cholesterol: TD 88137 Envigo).
547 Bone marrow chimeras were generated by treating ApoE$^{-/-}$ mice that had been on high- fat diet

548 for 4 weeks with 20mg/kg of pharmaceutical grade busulfan for 5 days (total dose of 100mg/kg).
549 On day 6 mice were i.v. injected with 2.5-3 x 10^6 bone marrow cells from either 10-week *S.*
550 *mansoni* infected or control uninfected $ApoE^{-/-}$ mice on high-fat diet. Reconstitution was
551 validated via flow-cytometry at 3-weeks post-transfer and recipient mice were maintained on
552 high-fat diet for 10-weeks post-reconstitution.
553

554 ***S. mansoni* infection and glucose tolerance test**

555 $ApoE^{-/-}$ female and male mice of 6 weeks of age were exposed percutaneously to 90 cercariae of
556 *S. mansoni* or were mocked infected (as controls). At five- and ten-weeks post-infection mice
557 were fasted for 5 hours and baseline blood glucose levels were obtained via lateral tail vein nick.
558 Mice were then administered a single intraperitoneal injection of glucose (2mg/g of body weight,
559 ultrapure glucose, Sigma G7528). Blood glucose levels were obtained at 20, 60, and 90 min post
560 injection. Individual data points obtained were analyzed by Area Under Curve (AUC).
561

562 **Mouse macrophage culture**

563 Mouse bone marrow-derived macrophages (BMDM) were generated as follows: bone marrow
564 cells were isolated by centrifugation of bones at >10,000 x g in a microcentrifuge tube for 15
565 seconds as previously described [81]. Cells were differentiated in M-CSF (20ng/mL, Peprotech,
566 Rocky Hill, NJ) in complete macrophage medium (CMM: RPMI1640, 10% FCS, 2mM L-
567 glutamine and 1 IU/mL Pen-Strep for 6 or 7 days. On the last day, cells
568 were harvested in Cellstripper cell dissociation reagent (Corning) were washed with CMM) and
569 prepared for downstream assays.
570

571 **Glycolytic and phospho-oxidative metabolism measurement (seahorse assay)**

572 BMDM from different conditions (uninfected controls or *S. mansoni* infected) were resuspended
573 at the same concentration in XF assay media supplemented with 5% FCS and 5mM glucose. The
574 day before the assay, the probe plate was calibrated and incubated at 37 C in a non-CO2
575 incubator. Resuspended cells were seeded at a concentration of $1.5x10^5$ cells per well and
576 incubated for 20-60 minutes in the Prep Station incubator (37 C non-CO2 incubator). Following
577 initial incubation, XF Running Media (XF assay media with 5% FCS and 10mM Glucose) were
578 dispensed into each well. OCR and ECAR were measured by an XF96 Seahorse Extracellular
579 Flux Analyzer following the manufacturer's instructions. For the seahorse assay, cells were
580 treated with oligomycin (1uM), FCCP (1.5uM), rotenone (100nM) and antimycin A (1uM). Each
581 condition was performed in 2-3 technical replicates. For determination of palmitate dependent
582 respiration, BSA-conjugated palmitate (BSA: palmitate = 1:6, molar ratio) was prepared
583 according to the Seahorse protocol (Seahorse Bioscience). Briefly, 1 mM sodium palmitate
584 (Sigma Aldrich) was conjugated with 0.17 mM fatty acid free-BSA (Sigma Aldrich) in 150 mM
585 NaCl solution at 37°C for 1h. Palmitate-BSA was stored in glass vials at -20°C until use. Cells
586 were incubated as above in glucose limited XF media per manufacturer instructions.

587

588 **Flow Cytometry**

589 Livers from uninfected and infected mice were perfused with 1X PBS, mashed and digested in
590 DMEM 0.5% Collagenase (Sigma) at 37°C for 15 min. Then, livers were mashed and filtered
591 through a 100 µm metal strainer and digested an additional 15 min. Following second digestion,
592 the liver contents were strained, washed with DMEM and spun down 1500 rpm for 5 min. The
593 pellet was lysed with 1X lysis buffer (BD PharmLyse), quenched with 1% FBS DMEM, and

594 washed to be used in flow cytometry. Surface staining was performed using the following mAb
595 against mouse antigens: CD45 (30-F11, eBioscience), CD301(BioRad), CD206 (C068C2,
596 Biolegend), F4/80 (BM8, Biolegend), mouse Mer biotinylated (R&D), CD64(X54-5/7.1, BD).
597 Intracellular antigen staining such as Nos2 (CXNFT, Invitrogen, and C-11, Santa Cruz) and Arg1
598 (Invitrogen, A1exF5)) was performed using the Intracellular Fixation and Permeabilization
599 Buffer set (Thermo Fisher Scientific cat. no. 88-8824) per manufacturer's instruction. Further,
600 bone marrow cells were obtained by centrifugation of bones into tubes at >10000 rpm for 15 s.
601 Surface staining for bone marrow precursors was performed using the following antibodies:
602 Ter119, CD19, CD4, CD3, Gr-1, CD11b, Sca-1, CD115, Ly6C, c-Kit, flt3, CD127 and CD16/32.
603 PBMC from whole blood were obtained following red blood cell lysis and used for flow
604 cytometry analysis. Surface staining of PBMC was performed using Ter119, CD64, CD11b,
605 CD115, Ly6C and MitoTracker Red.
606 Samples were acquired using Attune NxT Focusing Flow Cytometer (Thermo Fisher Scientific)
607 and analyzed using Flowjo X 10.0.7r2 (FlowJo LLC, Inc.).
608
609 **RNA Isolation and q-RT-PCR**
610 BMDM were stored in Trizol, and RNA isolation was performed as described in the
611 Immunological Genome Project Total RNA isolation protocol. Next, cDNA was synthesized
612 from RNA using Superscript IV VILO (ThermoFisher Scientific) for reverse transcription. qPCR
613 was performed using TaqMan Gene expression assays (Mgll, Slc1a3, beta actin, ThermoFisher)
614 on an Applied Biosystems Stepone Plus Real-Time PCR System. Beta-Actin assay number
615 Mm00607939_s1, mgll assay Mm00449274_m1, slc1a3 assay Mm00600697_m1. Relative
616 expression was calculated using the 2-ΔΔCt method.

617

618 **Measurement of Cytokines and Inflammatory mediators**

619 For cytokine levels of BMDCs, supernatants were collected at 24 hours post stimulation and
620 measured with Mouse Cytokine and Chemokine ProcartaPlex 26plex panel (Life Technologies)
621 per manufacture instructions using a Luminex Magpix system. Nitrite levels in cell culture media
622 were determined using a Griess reagent kit for nitrite determination (Invitrogen) according the
623 manufacturer's instructions.

624

625 **Untargeted lipidomics**

626 *Sample extraction from serum or cell pellets*

627 Lipids were extracted from serum (50µL) or cell pellets in a combined solution as described in
628 [82]. In detail, samples were combined in solution with 225 µL MeOH containing internal
629 standards (IS; Avanti splash Lipidomix (Lot#12), 10µL each sample) and 750 µL methyl tert-
630 butyl ether (MTBE). The samples were sonicated for 1 min, rested on ice for 1 hour, briefly
631 vortexed every 15 min then an addition of 200µL dd-H2O was made to induce phase separation.
632 All solutions were pre-chilled on ice. The sample were then vortexed for 20 s, rested at room
633 temperature for 10 min, and centrifuged at 14,000 g for 10 min at 4 C. The upper organic phase
634 was collected and evaporated to dryness under vacuum. Lipid samples were reconstituted in
635 200µL IPA and transferred to an LC-MS vial with insert for analysis. Concurrently, a process
636 blank sample was brought forward as well as quality control sample was prepared by taking
637 equal volumes (10µL per sample) from each sample after final resuspension.

638

639 *LC-MS Methods*

640 Lipid extracts were separated on a Waters Acquity UPLC CSH C18 1.7 um 2.1 x 100 mm
641 column maintained at 65 °C connected to an Agilent HiP 1290 Sampler, Agilent 1290 Infinity
642 pump, equipped with an Agilent 1290 Flex Cube and Agilent 6530 Accurate Mass Q-TOF dual
643 ESI mass spectrometer. For positive mode, the source gas temperature was set to 225 °C, with a
644 gas flow of 11 L/min and a nebulizer pressure of 50 psig. VCap voltage was set at 3500 V,
645 fragmentor at 110 V, skimmer at 85 V and Octopole RF peak at 750 V. For negative mode, the
646 source gas temperature was set at 325 °C, with a drying gas flow of 12 L/min and a nebulizer
647 pressure of 30 psig. VCap voltage is set 3000 V, fragmentor at125 V, skimmer at 75 V and
648 Octopole RF peak at 750 V. Reference masses in positive mode (*m/z* 121.0509 and 922.0098)
649 were infused with nebulizer pressure at 2 psig, in negative mode reference masses (*m/z*
650 1033.988, 966.0007, 112.9856 and 68.9958) were infused with a nebulizer pressure at 5psig.
651 Samples were analyzed in a randomized order in both positive and negative ionization modes in
652 separate experiments acquiring with the scan range m/z 100-1700. Mobile phase A consisted of
653 ACN:H_2O (60:40 *v/v*) in 10 mM ammonium formate and 0.1% formic acid, and mobile phase B
654 consisted of IPA:ACN:H_20 (90:9:1 *v/v*) in 10 mM ammonium formate and 0.1% formic acid.
655 The chromatography gradient for both positive and negative modes started at 15% mobile phase
656 B then increased to 30% B over 2.4 min, then increased to 48% from 2.4-3.0 min, followed by an
657 increase to 82% B from 3-13.2 min, and then to 99% from 13.2-13.8 min where it was held until
658 15.4 min and then returned to the initial conditioned and equilibrated for 4 min. Flow was 0.5
659 mL/min throughout, injection volume was 5μL for positive and 7 μL negative mode. Tandem
660 mass spectrometry is conducted using the same LC gradient at collision energies of 20 V and 40
661 V.
662

663 **Targeted lipidomics**

664 *Sample Preparation*

665 Lipids were extracted from cell pellets (500,000 cells) as described in detail above [82]. For
666 targeted lipidomics, lipid extracts were separated on a Waters BEH HILIC column 1.7 µm, 100
667 mm × 3 mm column maintained at 60 °C connected to an Agilent HiP 1290 Sampler, Agilent
668 1290 Infinity pump, and equipped with an Agilent 6490 triple quadrupole (QqQ) mass
669 spectrometer. Lipids were detected using dynamic multiple reaction monitoring (dMRM) in
670 negative ion mode. Source gas temperature is set to 225 °C, with a gas flow of 13 L/min and a
671 nebulizer pressure of 30 psi. Sheath gas temperature was 350 °C, sheath gas flow was 11 L/min,
672 capillary voltage of 4000 V, nozzle voltage was 500 V, high pressure RF was 190 V and low-
673 pressure RF was 120 V. Injection volume was 2 µL and the samples were injected in a
674 randomized order. Mobile phase A consisted of H_2O, mobile phase B consisted of ACN:H_2O
675 (96:4 *v/v*) and both contain 7 mM ammonium acetate. The chromatography gradient started at
676 100% mobile phase B and decreased to 84% B over 10 min. Post-time was 9 min and the flow
677 rate was 0.4 mL/min throughout. Collision energies (25 V) and cell accelerator voltages (3 V)
678 were optimized using lipid standards with dMRM quantifier transitions as $[M-H]^- \rightarrow [T2_RCOO]^-$
679 and qualifier transitions of $[M-H]^- \rightarrow [T1_RCOO]^-$ and $[M-H]^- \rightarrow [NL_T2Ketene]^-$.

680

681 **Lipid data analysis**

682 The pooled QC samples and process blank samples were injected throughout the sample queue to
683 ensure the reliability of acquired LC-MS data. Results from LC-MS experiments were collected
684 using Agilent MassHunter (MH) Workstation and analyzed using the software packages MH
685 Qual, MH Quant (Agilent Technologies, Inc) and LipidMatch to prepare the data set.

686 The data table exported from MHQuant was evaluated using Excel where initial lipid targets
687 were parsed based on the following criteria. Only lipids with relative standard deviation (RSD)
688 less than 30% in QC samples were used for data analysis. Additionally, targets identified in
689 blanks or double blanks at significant amounts (area under the curve (AUC) target blank/AUC
690 target QC >30%) were removed from analysis. Lipids were quantitated based on peak area ratios
691 to the spiked IS of the same or nearest class.
692
693 **RNA Sequencing**
694 Library Preparation and sequencing
695 The concentration and quality of total RNA samples was first assessed using Agilent 2100
696 Bioanalyzer. A RIN (RNA Integrity Number) of five or higher was required to pass the quality
697 control. Then 200 nanograms of RNA per sample were used to prepared dual-indexed strand-
698 specific cDNA library using KAPA mRNA Hyperprep Kit (Roche). The resulting libraries were
699 assessed for its quantity and size distribution using Qubit and Agilent 2100 Bioanalyzer. Two
700 hundred pico molar pooled libraries were utilized per flowcell for clustering amplification on
701 cBot using HiSeq 3000/4000 PE Cluster Kit and sequenced with 2.75bp paired-end configuration
702 on HiSeq4000 (Illumina) using HiSeq 3000/4000 PE SBS Kit. A Phred quality score (Q score)
703 was used to measure the quality of sequencing. More than 90% of the sequencing reads reached
704 Q30 (99.9% base call accuracy).
705
706 Sequence alignment and gene counts
707 The sequencing data were first assessed using FastQC (Babraham Bioinformatics, Cambridge,
708 UK) for quality control. Then all sequenced libraries were mapped to the mouse genome (UCSC

709 mm10) using STAR RNA-seq aligner [83] with the following parameter: "--
710 outSAMmapqUnique 60". The reads distribution across the genome was assessed using bamutils
711 (from ngsutils) [84]. Uniquely mapped sequencing reads were assigned to mm10 refGene genes
712 using featureCounts (from subread) [85] with the following parameters: "-s 2 –p –Q 10". Quality
713 control of sequencing and mapping results was summarized using MultiQC [86]. Genes with
714 read count per million (CPM) > 0.5 in more than 2 of the samples were kept. The data was
715 normalized using TMM (trimmed mean of M values) method. Differential expression analysis
716 was performed using edgeR [87, 88]. False discovery rate (FDR) was computed from p-values
717 using the Benjamini-Hochberg procedure.
718 Pathway analysis
719 The Data (significantly impacted pathways, biological processes, molecular interactions.) were
720 analyzed using Advaita Bio's iPathwayGuide (http://www.advaitabio.com/ipathwayguide).
721 Pathway analysis was performed on $\log_2$-transformed data using Bonferroni-corrected *p*-values.
722 The data discussed in this publication have been deposited in NCBI's Gene Expression Omnibus
723 (Edgar *et al*., 2002) and are accessible through GEO Series accession number GSE
724 144447(https://www.ncbi.nlm.nih.gov/geo/query/acc.cgi?acc=GSE144447)
725
726 **Heavy glucose and heavy palmitate labeling**
727 For metabolomics tracing in Figure 2 BMDM were differentiated in CMM containing normal
728 glucose. At Day 6 of culture cells were switched to CMM containing $^{13}C_6$-glucose (Santa Cruz
729 Biotech) for 24 hours. Cells were harvested and processed as described below. For metabolomics
730 tracing in figure 5 BMDM were differentiated in CMM containing normal glucose and serum. At

731 Day 6 of culture cells were switched to CMM containing dialyzed serum and 1 mM ^{13}C

732 palmitate (sigma Aldrich) for 36 hours. Cells were harvested and processed as described below.

733
734

735 **Metabolomics**

736 *Extraction*

737 Cold 90% methanol (MeOH) solution was added to each sample to give a final concentration of

738 80% MeOH to each cell pellet. Samples were incubated at -20 °C for 1 hr. After incubation, the

739 samples were centrifuged at 20,000 x g for 10 minutes at 4 °C. The supernatant was transferred

740 from each sample tube into a labeled, fresh micro centrifuge tube. The samples were dried *en*

741 *vacuo*.

742

743 *Mass Spectrometry Analysis of Samples*

744 All GC-MS analysis was performed with an Agilent 7200 GC-QTOF and an Agilent 7693A

745 automatic liquid sampler. Dried samples were suspended in 40 µL of a 40 mg/mL O-

746 methoxylamine hydrochloride (MOX) (MP Bio #155405) in dry pyridine (EMD Millipore

747 #PX2012-7) and incubated for one hour at 37 °C in a sand bath. 25 µL of this solution was

748 added to auto sampler vials followed by the automatic addition of 60 µL of N-methyl-N-

749 trimethylsilyltrifluoracetamide (MSTFA with 1%TMCS, Thermo #TS48913) and incubated for

750 30 minutes at 37 °C. Following incubation, each sample were vortexed and 1 µL of the prepared

751 sample was injected into the gas chromatograph inlet in the split mode with the inlet temperature

752 held at 250 °C. A 10:1 split ratio was used for analysis for the majority of metabolites. Any

753 metabolites that saturated the instrument at the 10:1 split was analyzed at a 50:1 split ratio. The

754 gas chromatograph had an initial temperature of 60 °C for one minute followed by a 10°C/min

755 ramp to 325 °C and a hold time of 10 minutes. A 30-meter Agilent Zorbax DB-5MS with 10 m
756 Duraguard capillary column was employed for chromatographic separation. Helium was used as
757 the carrier gas at a rate of 1 mL/min.
758
759 *Data Analysis*
760 The area under the curve for each isotope was extracted using MHQuant software (Agilent). This
761 data was exported as a .csv file and isotopically corrected using an in house modified version of
762 DeuteRater [89]
763
764 **Machine Learning**
765 The selection of the most informative or important features (i.e., the features contributing to the
766 prediction) was performed using a machine-learning approach involving an elastic-net regressor,
767 which followed a round of traditional univariate filtering. The process included two steps:
768 1. Creating a series of ANOVA models (one for each of the lipid-based features), and pre-
769 selecting features based on η^2 to limit the complexity of the downstream elastic net
770 model. The uninformative features were rejected and not used in the second step.
771 2. Establishing an elastic net regression model via cross-validation and grid-search of the
772 parameters. The zero coefficients of the model were removed. The top 20 non-zero
773 coefficients provided ranking for the features in terms of their importance.

774 The elastic net regression attempts to minimize the following functional:

775 $$\hat{\beta} = \underset{\beta}{\operatorname{argmin}}\left(\left|\left| y - X\beta \right|\right|^2 + \lambda\left((1-\alpha)\left|\left|\beta\right|\right|^2 / 2 + \alpha\left|\left|\beta\right|\right|_1 \right)\right)$$

over a grid of α and λ values [53]. The elastic-net approach linearly combines the L_1 and L_2 penalties used in LASSO [90] and ridge-regression methods [91], respectively. Therefore, the elastic net penalty would become LASSO penalty for $\alpha = 1$ and ridge penalty for $\alpha = 0$. The parameter λ controls the overall strength of the combined penalty term. The input X in the model consists of all the molecular features identified, and y is probability of observing a particular animal.

Statistical Analysis

Statistical analyses of data were performed using one-way ANOVA, a non-parametric Mann-Whitney test, or unpaired Student's t-test depending on the data distribution. $P \leq 0.05$ were considered statistically significant. Analyses and graphing were performed using Prism (GraphPad v8.0) and R-language for statistical computing.

References

1. Roth GA, Johnson C, Abajobir A, Abd-Allah F, Abera SF, Abyu G, et al. Global, Regional, and National Burden of Cardiovascular Diseases for 10 Causes, 1990 to 2015. J Am Coll Cardiol. 2017;70(1):1-25. Epub 2017/05/22. doi: 10.1016/j.jacc.2017.04.052. PubMed PMID: 28527533; PubMed Central PMCID: PMCPMC5491406.
2. Hinton W, McGovern A, Coyle R, Han TS, Sharma P, Correa A, et al. Incidence and prevalence of cardiovascular disease in English primary care: a cross-sectional and follow-up study of the Royal College of General Practitioners (RCGP) Research and Surveillance Centre (RSC). BMJ Open. 2018;8(8):e020282. Epub 2018/08/22. doi: 10.1136/bmjopen-2017-020282. PubMed PMID: 30127048; PubMed Central PMCID: PMCPMC6104756.
3. Emerging Risk Factors C, Sarwar N, Gao P, Seshasai SR, Gobin R, Kaptoge S, et al. Diabetes mellitus, fasting blood glucose concentration, and risk of vascular disease: a collaborative meta-analysis of 102 prospective studies. Lancet. 2010;375(9733):2215-22. Epub 2010/07/09. doi: 10.1016/S0140-6736(10)60484-9. PubMed PMID: 20609967; PubMed Central PMCID: PMCPMC2904878.

806 4. Marks JB, Raskin P. Cardiovascular risk in diabetes: a brief review. J Diabetes
807 Complications. 2000;14(2):108-15. Epub 2000/08/26. doi: 10.1016/s1056-8727(00)00065-9.
808 PubMed PMID: 10959073.
809 5. Wong ND, Zhao Y, Patel R, Patao C, Malik S, Bertoni AG, et al. Cardiovascular Risk Factor
810 Targets and Cardiovascular Disease Event Risk in Diabetes: A Pooling Project of the
811 Atherosclerosis Risk in Communities Study, Multi-Ethnic Study of Atherosclerosis, and Jackson
812 Heart Study. Diabetes Care. 2016;39(5):668-76. Epub 2016/05/22. doi: 10.2337/dc15-2439.
813 PubMed PMID: 27208374; PubMed Central PMCID: PMCPMC4839178.
814 6. Opotowsky AR, McWilliams JM, Cannon CP. Gender differences in aspirin use among
815 adults with coronary heart disease in the United States. J Gen Intern Med. 2007;22(1):55-61.
816 Epub 2007/03/14. doi: 10.1007/s11606-007-0116-5. PubMed PMID: 17351840; PubMed
817 Central PMCID: PMCPMC1824779.
818 7. Tan YY, Gast GC, van der Schouw YT. Gender differences in risk factors for coronary
819 heart disease. Maturitas. 2010;65(2):149-60. Epub 2009/11/10. doi:
820 10.1016/j.maturitas.2009.09.023. PubMed PMID: 19897327.
821 8. Humphries KH, Izadnegahdar M, Sedlak T, Saw J, Johnston N, Schenck-Gustafsson K, et
822 al. Sex differences in cardiovascular disease - Impact on care and outcomes. Front
823 Neuroendocrinol. 2017;46:46-70. Epub 2017/04/22. doi: 10.1016/j.yfrne.2017.04.001. PubMed
824 PMID: 28428055; PubMed Central PMCID: PMCPMC5506856.
825 9. Peters SA, Huxley RR, Woodward M. Diabetes as risk factor for incident coronary heart
826 disease in women compared with men: a systematic review and meta-analysis of 64 cohorts
827 including 858,507 individuals and 28,203 coronary events. Diabetologia. 2014;57(8):1542-51.
828 Epub 2014/05/27. doi: 10.1007/s00125-014-3260-6. PubMed PMID: 24859435.
829 10. Kim SH, Reaven G. Sex differences in insulin resistance and cardiovascular disease risk. J
830 Clin Endocrinol Metab. 2013;98(11):E1716-21. Epub 2013/09/26. doi: 10.1210/jc.2013-1166.
831 PubMed PMID: 24064694; PubMed Central PMCID: PMCPMC3816264.
832 11. Willeit J, Kiechl S, Egger G, Oberhollenzer M, Oberhollenzer F, Muggeo M, et al. The role
833 of insulin in age-related sex differences of cardiovascular risk profile and morbidity.
834 Atherosclerosis. 1997;130(1-2):183-9. Epub 1997/04/01. PubMed PMID: 9126663.
835 12. Moran A, Jacobs DR, Jr., Steinberger J, Steffen LM, Pankow JS, Hong CP, et al. Changes in
836 insulin resistance and cardiovascular risk during adolescence: establishment of differential risk
837 in males and females. Circulation. 2008;117(18):2361-8. Epub 2008/04/23. doi:
838 10.1161/CIRCULATIONAHA.107.704569. PubMed PMID: 18427135.
839 13. Cnop M, Havel PJ, Utzschneider KM, Carr DB, Sinha MK, Boyko EJ, et al. Relationship of
840 adiponectin to body fat distribution, insulin sensitivity and plasma lipoproteins: evidence for
841 independent roles of age and sex. Diabetologia. 2003;46(4):459-69. Epub 2003/04/11. doi:
842 10.1007/s00125-003-1074-z. PubMed PMID: 12687327.
843 14. Baars A, Oosting A, Lohuis M, Koehorst M, El Aidy S, Hugenholtz F, et al. Sex differences
844 in lipid metabolism are affected by presence of the gut microbiota. Sci Rep. 2018;8(1):13426.
845 Epub 2018/09/09. doi: 10.1038/s41598-018-31695-w. PubMed PMID: 30194317; PubMed
846 Central PMCID: PMCPMC6128923.
847 15. Stanley RG, Jackson CL, Griffiths K, Doenhoff MJ. Effects of Schistosoma mansoni worms
848 and eggs on circulating cholesterol and liver lipids in mice. Atherosclerosis. 2009;207(1):131-8.
849 doi: 10.1016/j.atherosclerosis.2009.04.037. PubMed PMID: 19464685.

850 16. Doenhoff MJ, Stanley RG, Griffiths K, Jackson CL. An anti-atherogenic effect of
851 Schistosoma mansoni infections in mice associated with a parasite-induced lowering of blood
852 total cholesterol. Parasitology. 2002;125(Pt 5):415-21. Epub 2002/12/03. PubMed PMID:
853 12458825.
854 17. Wiria AE, Hamid F, Wammes LJ, Prasetyani MA, Dekkers OM, May L, et al. Infection with
855 Soil-Transmitted Helminths Is Associated with Increased Insulin Sensitivity. PloS one.
856 2015;10(6):e0127746. doi: 10.1371/journal.pone.0127746. PubMed PMID: 26061042; PubMed
857 Central PMCID: PMCPMC4464734.
858 18. Wolfs IM, Stoger JL, Goossens P, Pottgens C, Gijbels MJ, Wijnands E, et al.
859 Reprogramming macrophages to an anti-inflammatory phenotype by helminth antigens
860 reduces murine atherosclerosis. FASEB J. 2014;28(1):288-99. Epub 2013/09/18. doi:
861 10.1096/fj.13-235911. PubMed PMID: 24043262.
862 19. Cortes-Selva D, Elvington AF, Ready A, Rajwa B, Pearce EJ, Randolph GJ, et al.
863 Schistosoma mansoni Infection-Induced Transcriptional Changes in Hepatic Macrophage
864 Metabolism Correlate With an Athero-Protective Phenotype. Front Immunol. 2018;9:2580.
865 Epub 2018/11/30. doi: 10.3389/fimmu.2018.02580. PubMed PMID: 30483256; PubMed Central
866 PMCID: PMCPMC6240656.
867 20. Chen Y, Lu J, Huang Y, Wang T, Xu Y, Xu M, et al. Association of previous schistosome
868 infection with diabetes and metabolic syndrome: a cross-sectional study in rural China. The
869 Journal of clinical endocrinology and metabolism. 2013;98(2):E283-7. doi: 10.1210/jc.2012-
870 2517. PubMed PMID: 23275524.
871 21. Sanya RE, Webb EL, Zziwa C, Kizindo R, Sewankambo M, Tumusiime J, et al. The effect of
872 helminth infections and their treatment on metabolic outcomes: results of a cluster-
873 randomised trial. Clinical infectious diseases : an official publication of the Infectious Diseases
874 Society of America. 2019. Epub 2019/09/11. doi: 10.1093/cid/ciz859. PubMed PMID: 31504336.
875 22. Shen SW, Lu Y, Li F, Shen ZH, Xu M, Yao WF, et al. The potential long-term effect of
876 previous schistosome infection reduces the risk of metabolic syndrome among Chinese men.
877 Parasite immunology. 2015;37(7):333-9. Epub 2015/03/27. doi: 10.1111/pim.12187. PubMed
878 PMID: 25809087.
879 23. Wolde M, Berhe N, Medhin G, Chala F, van Die I, Tsegaye A. Inverse Associations of
880 Schistosoma mansoni Infection and Metabolic Syndromes in Humans: A Cross-Sectional Study
881 in Northeast Ethiopia. Microbiol Insights. 2019;12:1178636119849934. Epub 2019/06/18. doi:
882 10.1177/1178636119849934. PubMed PMID: 31205419; PubMed Central PMCID:
883 PMCPMC6537292.
884 24. Barron L, Wynn TA. Macrophage activation governs schistosomiasis-induced
885 inflammation and fibrosis. European journal of immunology. 2011;41(9):2509-14. Epub
886 2011/09/29. doi: 10.1002/eji.201141869. PubMed PMID: 21952807; PubMed Central PMCID:
887 PMC3408543.
888 25. Fairfax KC, Everts B, Smith AM, Pearce EJ. Regulation of the development of the hepatic
889 B cell compartment during Schistosoma mansoni infection. J Immunol. 2013;191(8):4202-10.
890 Epub 2013/09/17. doi: 10.4049/jimmunol.1301357. PubMed PMID: 24038090; PubMed Central
891 PMCID: PMC3851305.
892 26. Herbert DR, Holscher C, Mohrs M, Arendse B, Schwegmann A, Radwanska M, et al.
893 Alternative macrophage activation is essential for survival during schistosomiasis and

894 downmodulates T helper 1 responses and immunopathology. Immunity. 2004;20(5):623-35.
895 Epub 2004/05/15. PubMed PMID: 15142530.
896 27. Vats D, Mukundan L, Odegaard JI, Zhang L, Smith KL, Morel CR, et al. Oxidative
897 metabolism and PGC-1beta attenuate macrophage-mediated inflammation. Cell Metab.
898 2006;4(1):13-24. doi: 10.1016/j.cmet.2006.05.011. PubMed PMID: 16814729; PubMed Central
899 PMCID: PMCPMC1904486.
900 28. Huang SC, Everts B, Ivanova Y, O'Sullivan D, Nascimento M, Smith AM, et al. Cell-intrinsic
901 lysosomal lipolysis is essential for alternative activation of macrophages. Nature immunology.
902 2014;15(9):846-55. doi: 10.1038/ni.2956. PubMed PMID: 25086775; PubMed Central PMCID:
903 PMCPMC4139419.
904 29. Ng MK, Jessup W, Celermajer DS. Sex-related differences in the regulation of
905 macrophage cholesterol metabolism. Curr Opin Lipidol. 2001;12(5):505-10. Epub 2001/09/19.
906 PubMed PMID: 11561169.
907 30. Griffin C, Lanzetta N, Eter L, Singer K. Sexually dimorphic myeloid inflammatory and
908 metabolic responses to diet-induced obesity. American journal of physiology Regulatory,
909 integrative and comparative physiology. 2016;311(2):R211-6. Epub 2016/06/03. doi:
910 10.1152/ajpregu.00136.2016. PubMed PMID: 27252473; PubMed Central PMCID:
911 PMCPMC5008668.
912 31. Rudyk MP, Pozur VV, Voieikova DO, Hurmach YV, Khranovska NM, Skachkova OV, et al.
913 Sex-based differences in phagocyte metabolic profile in rats with monosodium glutamate-
914 induced obesity. Sci Rep. 2018;8(1):5419. Epub 2018/04/05. doi: 10.1038/s41598-018-23664-0.
915 PubMed PMID: 29615659; PubMed Central PMCID: PMCPMC5882925.
916 32. Taneja V. Sex Hormones Determine Immune Response. Front Immunol. 2018;9:1931.
917 Epub 2018/09/14. doi: 10.3389/fimmu.2018.01931. PubMed PMID: 30210492; PubMed Central
918 PMCID: PMCPMC6119719.
919 33. Rubinow KB. An intracrine view of sex steroids, immunity, and metabolic regulation. Mol
920 Metab. 2018;15:92-103. Epub 2018/03/20. doi: 10.1016/j.molmet.2018.03.001. PubMed PMID:
921 29551633; PubMed Central PMCID: PMCPMC6066741.
922 34. Winn NC, Jurrissen TJ, Grunewald ZI, Cunningham RP, Woodford ML, Kanaley JA, et al.
923 Estrogen receptor-alpha signaling maintains immunometabolic function in males and is
924 obligatory for exercise-induced amelioration of nonalcoholic fatty liver. Am J Physiol Endocrinol
925 Metab. 2019;316(2):E156-E67. Epub 2018/12/05. doi: 10.1152/ajpendo.00259.2018. PubMed
926 PMID: 30512987; PubMed Central PMCID: PMCPMC6397364.
927 35. Potteaux S, Gautier EL, Hutchison SB, van Rooijen N, Rader DJ, Thomas MJ, et al.
928 Suppressed monocyte recruitment drives macrophage removal from atherosclerotic plaques of
929 Apoe-/- mice during disease regression. The Journal of clinical investigation. 2011;121(5):2025-
930 36. doi: 10.1172/JCI43802. PubMed PMID: 21505265; PubMed Central PMCID:
931 PMCPMC3083793.
932 36. Tacke F, Alvarez D, Kaplan TJ, Jakubzick C, Spanbroek R, Llodra J, et al. Monocyte subsets
933 differentially employ CCR2, CCR5, and CX3CR1 to accumulate within atherosclerotic plaques.
934 The Journal of clinical investigation. 2007;117(1):185-94. doi: 10.1172/JCI28549. PubMed PMID:
935 17200718; PubMed Central PMCID: PMCPMC1716202.
936 37. Rull A, Camps J, Alonso-Villaverde C, Joven J. Insulin resistance, inflammation, and
937 obesity: role of monocyte chemoattractant protein-1 (or CCL2) in the regulation of metabolism.

938 Mediators Inflamm. 2010;2010. Epub 2010/10/12. doi: 10.1155/2010/326580. PubMed PMID:
939 20936118; PubMed Central PMCID: PMCPMC2948922.
940 38. Beliard S, Le Goff W, Saint-Charles F, Poupel L, Deswaerte V, Bouchareychas L, et al.
941 Modulation of Gr1(low) monocyte subset impacts insulin sensitivity and weight gain upon high-
942 fat diet in female mice. Int J Obes (Lond). 2017;41(12):1805-14. Epub 2017/08/05. doi:
943 10.1038/ijo.2017.179. PubMed PMID: 28769122; PubMed Central PMCID: PMCPMC5729349.
944 39. Oh DY, Morinaga H, Talukdar S, Bae EJ, Olefsky JM. Increased macrophage migration
945 into adipose tissue in obese mice. Diabetes. 2012;61(2):346-54. Epub 2011/12/23. doi:
946 10.2337/db11-0860. PubMed PMID: 22190646; PubMed Central PMCID: PMCPMC3266418.
947 40. Liang CP, Han S, Senokuchi T, Tall AR. The macrophage at the crossroads of insulin
948 resistance and atherosclerosis. Circ Res. 2007;100(11):1546-55. Epub 2007/06/09. doi:
949 10.1161/CIRCRESAHA.107.152165. PubMed PMID: 17556668.
950 41. Pike Winer LS, Wu M. Rapid analysis of glycolytic and oxidative substrate flux of cancer
951 cells in a microplate. PLoS One. 2014;9(10):e109916. Epub 2014/11/02. doi:
952 10.1371/journal.pone.0109916. PubMed PMID: 25360519; PubMed Central PMCID:
953 PMCPMC4215881.
954 42. Liu PS, Wang H, Li X, Chao T, Teav T, Christen S, et al. alpha-ketoglutarate orchestrates
955 macrophage activation through metabolic and epigenetic reprogramming. Nat Immunol.
956 2017;18(9):985-94. Epub 2017/07/18. doi: 10.1038/ni.3796. PubMed PMID: 28714978.
957 43. Mehlem A, Hagberg CE, Muhl L, Eriksson U, Falkevall A. Imaging of neutral lipids by oil
958 red O for analyzing the metabolic status in health and disease. Nat Protoc. 2013;8(6):1149-54.
959 Epub 2013/05/25. doi: 10.1038/nprot.2013.055. PubMed PMID: 23702831.
960 44. Langston PK, Shibata M, Horng T. Metabolism Supports Macrophage Activation. Front
961 Immunol. 2017;8:61. Epub 2017/02/16. doi: 10.3389/fimmu.2017.00061. PubMed PMID:
962 28197151; PubMed Central PMCID: PMCPMC5281575.
963 45. Jung SB, Choi MJ, Ryu D, Yi HS, Lee SE, Chang JY, et al. Reduced oxidative capacity in
964 macrophages results in systemic insulin resistance. Nat Commun. 2018;9(1):1551. Epub
965 2018/04/21. doi: 10.1038/s41467-018-03998-z. PubMed PMID: 29674655; PubMed Central
966 PMCID: PMCPMC5908799.
967 46. Cortes-Selva D, Elvington AF, Ready A, Rajwa B, Pearce EJ, Randolph GJ, et al.
968 Schistosoma mansoni Infection-Induced Transcriptional Changes in Hepatic Macrophage
969 Metabolism Correlate With an Athero-Protective Phenotype. Frontiers in Immunology.
970 2018;9(2580). doi: 10.3389/fimmu.2018.02580.
971 47. Berdan CA, Erion KA, Burritt NE, Corkey BE, Deeney JT. Inhibition of Monoacylglycerol
972 Lipase Activity Decreases Glucose-Stimulated Insulin Secretion in INS-1 (832/13) Cells and Rat
973 Islets. PloS one. 2016;11(2):e0149008. Epub 2016/02/13. doi: 10.1371/journal.pone.0149008.
974 PubMed PMID: 26867016; PubMed Central PMCID: PMCPMC4750965.
975 48. Douglass JD, Zhou YX, Wu A, Zadroga JA, Gajda AM, Lackey AI, et al. Global deletion of
976 MGL in mice delays lipid absorption and alters energy homeostasis and diet-induced obesity. J
977 Lipid Res. 2015;56(6):1153-71. Epub 2015/04/07. doi: 10.1194/jlr.M058586. PubMed PMID:
978 25842377; PubMed Central PMCID: PMCPMC4442873.
979 49. Chella Krishnan K, Mehrabian M, Lusis AJ. Sex differences in metabolism and
980 cardiometabolic disorders. Curr Opin Lipidol. 2018;29(5):404-10. Epub 2018/08/30. doi:

981 10.1097/MOL.0000000000000536. PubMed PMID: 30156571; PubMed Central PMCID:
982 PMCPMC6382080.
983 50. Girgis NM, Gundra UM, Ward LN, Cabrera M, Frevert U, Loke P. Ly6C(high) monocytes
984 become alternatively activated macrophages in schistosome granulomas with help from CD4+
985 cells. PLoS pathogens. 2014;10(6):e1004080. doi: 10.1371/journal.ppat.1004080. PubMed
986 PMID: 24967715; PubMed Central PMCID: PMCPMC4072804.
987 51. Nascimento M, Huang SC, Smith A, Everts B, Lam W, Bassity E, et al. Ly6Chi monocyte
988 recruitment is responsible for Th2 associated host-protective macrophage accumulation in liver
989 inflammation due to schistosomiasis. PLoS pathogens. 2014;10(8):e1004282. doi:
990 10.1371/journal.ppat.1004282. PubMed PMID: 25144366; PubMed Central PMCID:
991 PMCPMC4140849.
992 52. Paul F, Arkin Y, Giladi A, Jaitin DA, Kenigsberg E, Keren-Shaul H, et al. Transcriptional
993 Heterogeneity and Lineage Commitment in Myeloid Progenitors. Cell. 2016;164(1-2):325. Epub
994 2016/01/14. doi: 10.1016/j.cell.2015.12.046. PubMed PMID: 28915372.
995 53. Zou HaH, T. Regularization and variable selection via the elastic net. Journal of the Royal
996 Statistical Society. 2005;67(2):301-20. doi: 10.1111/j.1467-9868.2005.00503.x.
997 54. Luquain-Costaz C, Lefai E, Arnal-Levron M, Markina D, Sakai S, Euthine V, et al.
998 Bis(monoacylglycero)phosphate accumulation in macrophages induces intracellular cholesterol
999 redistribution, attenuates liver-X receptor/ATP-Binding cassette transporter A1/ATP-binding
1000 cassette transporter G1 pathway, and impairs cholesterol efflux. Arterioscler Thromb Vasc Biol.
1001 2013;33(8):1803-11. Epub 2013/06/22. doi: 10.1161/ATVBAHA.113.301857. PubMed PMID:
1002 23788762; PubMed Central PMCID: PMCPMC3989212.
1003 55. Anheuser S, Breiden B, Sandhoff K. Membrane lipids and their degradation compounds
1004 control GM2 catabolism at intralysosomal luminal vesicles. J Lipid Res. 2019;60(6):1099-111.
1005 Epub 2019/04/17. doi: 10.1194/jlr.M092551. PubMed PMID: 30988135; PubMed Central
1006 PMCID: PMCPMC6547633.
1007 56. Funk JL, Feingold KR, Moser AH, Grunfeld C. Lipopolysaccharide stimulation of RAW
1008 264.7 macrophages induces lipid accumulation and foam cell formation. Atherosclerosis.
1009 1993;98(1):67-82. Epub 1993/01/04. doi: 10.1016/0021-9150(93)90224-i. PubMed PMID:
1010 8457252.
1011 57. Oiknine J, Aviram M. Increased susceptibility to activation and increased uptake of low
1012 density lipoprotein by cholesterol-loaded macrophages. Arterioscler Thromb. 1992;12(6):745-
1013 53. Epub 1992/06/01. doi: 10.1161/01.atv.12.6.745. PubMed PMID: 1591234.
1014 58. Carroll RG, Zaslona Z, Galvan-Pena S, Koppe EL, Sevin DC, Angiari S, et al. An unexpected
1015 link between fatty acid synthase and cholesterol synthesis in proinflammatory macrophage
1016 activation. The Journal of biological chemistry. 2018;293(15):5509-21. Epub 2018/02/22. doi:
1017 10.1074/jbc.RA118.001921. PubMed PMID: 29463677; PubMed Central PMCID:
1018 PMCPMC5900750.
1019 59. Vernia S, Cavanagh-Kyros J, Barrett T, Jung DY, Kim JK, Davis RJ. Diet-induced obesity
1020 mediated by the JNK/DIO2 signal transduction pathway. Genes Dev. 2013;27(21):2345-55. Epub
1021 2013/11/05. doi: 10.1101/gad.223800.113. PubMed PMID: 24186979; PubMed Central PMCID:
1022 PMCPMC3828520.
1023 60. Kurylowicz A, Jonas M, Lisik W, Jonas M, Wicik ZA, Wierzbicki Z, et al. Obesity is
1024 associated with a decrease in expression but not with the hypermethylation of thermogenesis-

1025 related genes in adipose tissues. J Transl Med. 2015;13:31. Epub 2015/01/28. doi:
1026 10.1186/s12967-015-0395-2. PubMed PMID: 25622596; PubMed Central PMCID:
1027 PMCPMC4314800.
1028 61. van der Windt GJ, Everts B, Chang CH, Curtis JD, Freitas TC, Amiel E, et al. Mitochondrial
1029 respiratory capacity is a critical regulator of CD8+ T cell memory development. Immunity.
1030 2012;36(1):68-78. Epub 2011/12/31. doi: 10.1016/j.immuni.2011.12.007. PubMed PMID:
1031 22206904; PubMed Central PMCID: PMCPMC3269311.
1032 62. Kannan Y, Perez-Lloret J, Li Y, Entwistle LJ, Khoury H, Papoutsopoulou S, et al. TPL-2
1033 Regulates Macrophage Lipid Metabolism and M2 Differentiation to Control TH2-Mediated
1034 Immunopathology. PLoS pathogens. 2016;12(8):e1005783. Epub 2016/08/04. doi:
1035 10.1371/journal.ppat.1005783. PubMed PMID: 27487182; PubMed Central PMCID:
1036 PMCPMC4972396.
1037 63. Garaude J, Acin-Perez R, Martinez-Cano S, Enamorado M, Ugolini M, Nistal-Villan E, et
1038 al. Mitochondrial respiratory-chain adaptations in macrophages contribute to antibacterial host
1039 defense. Nature immunology. 2016;17(9):1037-45. Epub 2016/06/28. doi: 10.1038/ni.3509.
1040 PubMed PMID: 27348412; PubMed Central PMCID: PMCPMC4994870.
1041 64. Puleston DJ, Buck MD, Klein Geltink RI, Kyle RL, Caputa G, O'Sullivan D, et al. Polyamines
1042 and eIF5A Hypusination Modulate Mitochondrial Respiration and Macrophage Activation. Cell
1043 Metab. 2019;30(2):352-63 e8. Epub 2019/05/28. doi: 10.1016/j.cmet.2019.05.003. PubMed
1044 PMID: 31130465; PubMed Central PMCID: PMCPMC6688828.
1045 65. Galvan-Pena S, O'Neill LA. Metabolic reprograming in macrophage polarization. Front
1046 Immunol. 2014;5:420. Epub 2014/09/18. doi: 10.3389/fimmu.2014.00420. PubMed PMID:
1047 25228902; PubMed Central PMCID: PMCPMC4151090.
1048 66. Shi L, Pan H, Liu Z, Xie J, Han W. Roles of PFKFB3 in cancer. Signal Transduct Target Ther.
1049 2017;2:17044. Epub 2017/12/22. doi: 10.1038/sigtrans.2017.44. PubMed PMID: 29263928;
1050 PubMed Central PMCID: PMCPMC5701083.
1051 67. Lam RS, O'Brien-Simpson NM, Holden JA, Lenzo JC, Fong SB, Reynolds EC. Unprimed, M1
1052 and M2 Macrophages Differentially Interact with Porphyromonas gingivalis. PloS one.
1053 2016;11(7):e0158629. Epub 2016/07/08. doi: 10.1371/journal.pone.0158629. PubMed PMID:
1054 27383471; PubMed Central PMCID: PMCPMC4934774.
1055 68. Boisvert WA, Rose DM, Johnson KA, Fuentes ME, Lira SA, Curtiss LK, et al. Up-regulated
1056 expression of the CXCR2 ligand KC/GRO-alpha in atherosclerotic lesions plays a central role in
1057 macrophage accumulation and lesion progression. The American journal of pathology.
1058 2006;168(4):1385-95. Epub 2006/03/28. doi: 10.2353/ajpath.2006.040748. PubMed PMID:
1059 16565511; PubMed Central PMCID: PMCPMC1606562.
1060 69. Zhou Z, Subramanian P, Sevilmis G, Globke B, Soehnlein O, Karshovska E, et al.
1061 Lipoprotein-derived lysophosphatidic acid promotes atherosclerosis by releasing CXCL1 from
1062 the endothelium. Cell Metab. 2011;13(5):592-600. Epub 2011/05/03. doi:
1063 10.1016/j.cmet.2011.02.016. PubMed PMID: 21531341.
1064 70. Nunemaker CS, Chung HG, Verrilli GM, Corbin KL, Upadhye A, Sharma PR. Increased
1065 serum CXCL1 and CXCL5 are linked to obesity, hyperglycemia, and impaired islet function. J
1066 Endocrinol. 2014;222(2):267-76. Epub 2014/06/15. doi: 10.1530/JOE-14-0126. PubMed PMID:
1067 24928936; PubMed Central PMCID: PMCPMC4135511.

1068 71. Qu D, Liu J, Lau CW, Huang Y. IL-6 in diabetes and cardiovascular complications. British
1069 journal of pharmacology. 2014;171(15):3595-603. Epub 2014/04/05. doi: 10.1111/bph.12713.
1070 PubMed PMID: 24697653; PubMed Central PMCID: PMCPMC4128059.
1071 72. Hartman J, Frishman WH. Inflammation and atherosclerosis: a review of the role of
1072 interleukin-6 in the development of atherosclerosis and the potential for targeted drug therapy.
1073 Cardiol Rev. 2014;22(3):147-51. Epub 2014/03/13. doi: 10.1097/CRD.0000000000000021.
1074 PubMed PMID: 24618929.
1075 73. Kaufmann E, Sanz J, Dunn JL, Khan N, Mendonca LE, Pacis A, et al. BCG Educates
1076 Hematopoietic Stem Cells to Generate Protective Innate Immunity against Tuberculosis. Cell.
1077 2018;172(1-2):176-90 e19. Epub 2018/01/13. doi: 10.1016/j.cell.2017.12.031. PubMed PMID:
1078 29328912.
1079 74. Hoogeveen RM, Nahrendorf M, Riksen NP, Netea MG, de Winther MPJ, Lutgens E, et al.
1080 Monocyte and haematopoietic progenitor reprogramming as common mechanism underlying
1081 chronic inflammatory and cardiovascular diseases. Eur Heart J. 2018;39(38):3521-7. Epub
1082 2017/10/27. doi: 10.1093/eurheartj/ehx581. PubMed PMID: 29069365; PubMed Central
1083 PMCID: PMCPMC6174026.
1084 75. Leentjens J, Bekkering S, Joosten LAB, Netea MG, Burgner DP, Riksen NP. Trained Innate
1085 Immunity as a Novel Mechanism Linking Infection and the Development of Atherosclerosis. Circ
1086 Res. 2018;122(5):664-9. Epub 2018/01/26. doi: 10.1161/CIRCRESAHA.117.312465. PubMed
1087 PMID: 29367213.
1088 76. Cheng SC, Quintin J, Cramer RA, Shepardson KM, Saeed S, Kumar V, et al. mTOR- and
1089 HIF-1alpha-mediated aerobic glycolysis as metabolic basis for trained immunity. Science.
1090 2014;345(6204):1250684. Epub 2014/09/27. doi: 10.1126/science.1250684. PubMed PMID:
1091 25258083; PubMed Central PMCID: PMCPMC4226238.
1092 77. Stienstra R, Netea-Maier RT, Riksen NP, Joosten LAB, Netea MG. Specific and Complex
1093 Reprogramming of Cellular Metabolism in Myeloid Cells during Innate Immune Responses. Cell
1094 Metab. 2017;26(1):142-56. Epub 2017/07/07. doi: 10.1016/j.cmet.2017.06.001. PubMed PMID:
1095 28683282.
1096 78. Ifrim DC, Quintin J, Joosten LA, Jacobs C, Jansen T, Jacobs L, et al. Trained immunity or
1097 tolerance: opposing functional programs induced in human monocytes after engagement of
1098 various pattern recognition receptors. Clin Vaccine Immunol. 2014;21(4):534-45. Epub
1099 2014/02/14. doi: 10.1128/CVI.00688-13. PubMed PMID: 24521784; PubMed Central PMCID:
1100 PMCPMC3993125.
1101 79. Christ A, Gunther P, Lauterbach MAR, Duewell P, Biswas D, Pelka K, et al. Western Diet
1102 Triggers NLRP3-Dependent Innate Immune Reprogramming. Cell. 2018;172(1-2):162-75 e14.
1103 Epub 2018/01/13. doi: 10.1016/j.cell.2017.12.013. PubMed PMID: 29328911; PubMed Central
1104 PMCID: PMCPMC6324559.
1105 80. Krenkel O, Hundertmark J, Abdallah AT, Kohlhepp M, Puengel T, Roth T, et al. Myeloid
1106 cells in liver and bone marrow acquire a functionally distinct inflammatory phenotype during
1107 obesity-related steatohepatitis. Gut. 2020;69(3):551-63. Epub 2019/05/12. doi: 10.1136/gutjnl-
1108 2019-318382. PubMed PMID: 31076404.
1109 81. Amend SR, Valkenburg KC, Pienta KJ. Murine Hind Limb Long Bone Dissection and Bone
1110 Marrow Isolation. J Vis Exp. 2016;(110). Epub 2016/05/12. doi: 10.3791/53936. PubMed PMID:
1111 27168390; PubMed Central PMCID: PMCPMC4941920.

1112 82. Matyash V, Liebisch G, Kurzchalia TV, Shevchenko A, Schwudke D. Lipid extraction by
1113 methyl-tert-butyl ether for high-throughput lipidomics. J Lipid Res. 2008;49(5):1137-46. Epub
1114 2008/02/19. doi: 10.1194/jlr.D700041-JLR200. PubMed PMID: 18281723; PubMed Central
1115 PMCID: PMCPMC2311442.
1116 83. Dobin A, Davis CA, Schlesinger F, Drenkow J, Zaleski C, Jha S, et al. STAR: ultrafast
1117 universal RNA-seq aligner. Bioinformatics. 2013;29(1):15-21. Epub 2012/10/30. doi:
1118 10.1093/bioinformatics/bts635. PubMed PMID: 23104886; PubMed Central PMCID:
1119 PMCPMC3530905.
1120 84. Breese MR, Liu Y. NGSUtils: a software suite for analyzing and manipulating next-
1121 generation sequencing datasets. Bioinformatics. 2013;29(4):494-6. Epub 2013/01/15. doi:
1122 10.1093/bioinformatics/bts731. PubMed PMID: 23314324; PubMed Central PMCID:
1123 PMCPMC3570212.
1124 85. Liao Y, Smyth GK, Shi W. featureCounts: an efficient general purpose program for
1125 assigning sequence reads to genomic features. Bioinformatics. 2014;30(7):923-30. Epub
1126 2013/11/15. doi: 10.1093/bioinformatics/btt656. PubMed PMID: 24227677.
1127 86. Ewels P, Magnusson M, Lundin S, Kaller M. MultiQC: summarize analysis results for
1128 multiple tools and samples in a single report. Bioinformatics. 2016;32(19):3047-8. Epub
1129 2016/06/18. doi: 10.1093/bioinformatics/btw354. PubMed PMID: 27312411; PubMed Central
1130 PMCID: PMCPMC5039924.
1131 87. Robinson MD, McCarthy DJ, Smyth GK. edgeR: a Bioconductor package for differential
1132 expression analysis of digital gene expression data. Bioinformatics. 2010;26(1):139-40. Epub
1133 2009/11/17. doi: 10.1093/bioinformatics/btp616. PubMed PMID: 19910308; PubMed Central
1134 PMCID: PMCPMC2796818.
1135 88. McCarthy DJ, Chen Y, Smyth GK. Differential expression analysis of multifactor RNA-Seq
1136 experiments with respect to biological variation. Nucleic Acids Res. 2012;40(10):4288-97. Epub
1137 2012/01/31. doi: 10.1093/nar/gks042. PubMed PMID: 22287627; PubMed Central PMCID:
1138 PMCPMC3378882.
1139 89. Naylor BC, Porter MT, Wilson E, Herring A, Lofthouse S, Hannemann A, et al.
1140 DeuteRater: a tool for quantifying peptide isotope precision and kinetic proteomics.
1141 Bioinformatics. 2017;33(10):1514-20. Epub 2017/01/18. doi: 10.1093/bioinformatics/btx009.
1142 PubMed PMID: 28093409.
1143 90. Tibshirani R. Regression shrinkage and selection via the lasso. J R Statist Soc B.
1144 1996;58:267–88. doi: 10.1111/j.2517-6161.1996.tb02080.x.
1145 91. Hoerl AaK, RW. Ridge Regression: Biased Estimation for Nonorthogonal Problems.
1146 Technometrics. 1970;12(1):55-67.
1147
1148
1149 **Figure legends**

1150 **Figure 1. Bone marrow derived macrophages (BMDM) from ApoE$^{-/-}$ male *S. mansoni***

1151 **infected mice exhibit increased oxygen consumption and mitochondria mass.** ApoE$^{-/-}$ male

1152 were fed HFD for 10 days before infection with *S. mansoni*. Ten weeks post infection mice were

1153 sacrificed and bone marrow cells were harvested and cultured for 7 days under M-CSF. (A)
1154 SeaHorse assay results for OCR of BMDC from infected and uninfected ApoE$^{-/-}$ males in basal
1155 conditions and in response to mitochondrial inhibitors. (B) Quantification (in picomoles per
1156 minute) of the basal oxygen consumption of BMDM from uninfected or infected ApoE$^{-/-}$ HFD
1157 male mice. (C) Quantification of the spare respiratory capacity of BMDM from uninfected or
1158 infected ApoE$^{-/-}$ HFD male mice (D) Extracellular acidification rate of BMDM from male
1159 uninfected or infected ApoE$^{-/-}$. (E) Oil Red O relative staining in BMDM from ApoE$^{-/-}$ mice (F)
1160 MitoTracker Red Deep Stain measure by flow cytometry in BMDM from ApoE$^{-/-}$ mice.
1161 SeaHorse assay analysis were performed the Seahorse XFe96 instrument. *$p < 0.05$; **$p < 0.01$;
1162 ***$p < 0.001$. Graphs are representative of multiple experiments (2-3), with n>4 per group.
1163
1164 Figure 2.
1165 **BMDM from male *S. mansoni* infected HFD ApoE$^{-/-}$ mice have increased TCA cycle usage**
1166 **and significantly reduced cholesterol esters.** A-E) Mϕ were differentiated from bone marrow
1167 of 10-week infected animals with M-CSF in a 7-day culture in normal glucose and then switched
1168 to ^{13}C-labeled glucose for 24 hours. F-H) Mϕs were differentiated with M-CSF in a 7-day culture
1169 and then total cellular lipids were extracted and analyzed via LC-MS based lipidomic analysis.
1170 F) PLS-DA derived score from HFD Infected and HFD Uninfected BMDM. G) Plot of lipid
1171 species from the BMDM of infected and uninfected males on HFD, significantly altered lipid
1172 species are red and labeled. H)Table of statistical analysis of VIP I) Box whisker plot of
1173 normalized AUC of cholesterol ester species, which were identified as VIP compounds from the
1174 PLS-DA analysis. J-L) Bone marrow macrophages were differentiated with M-CSF and mRNA
1175 sequenced via RNASeq. J) Volcano plot of significantly differentially expressed genes between
1176 BMDM from *S. mansoni* infected uninfected mice. K) iPathway analysis showed distinct profiles

1177 in BMDM from *S. mansoni* infected, mice. L,M) Total RNA was extracted from biologically
1178 independent BMDM differentiated in M-CSF for Real-time PCR validation of mgll and slc1a3
1179 regulation.
1180 Data in A-I are representative of 3 experiments with 4-6 mice per group in each experiment.
1181 Data in J and K are representative of sequencing of 2 biologically independent experiments with
1182 5-6 mice per group. Data in L are from 2 biologically independent experiments with 4-6 mice per
1183 group.
1184
1185 Figure 3
1186 ***S. mansoni* infection does not protect females from metabolic disease despite inducing**
1187 **alternative activation in hepatic macrophages**. (A-B) Total body weight and glucose tolerance
1188 test (GTT) at 10 weeks post-infection. GTT values were analyzed by Area Under the Curve and
1189 graphed using GraphPad Prims. (C) (D) Flow cytometry analysis of alternative activation
1190 markers CD206 and CD302 in perfused and digested livers gated on hepatic macrophages
1191 ($CD45^{+}CD64^{+}MertK^{+}$) Arg-1 expression in hepatic macrophages from uninfected and infected
1192 $ApoE^{-/-}$ mice Nos-2 expression by flow cytometry in hepatic macrophages 10 weeks post
1193 infection. (E) Ly6C expression in monocyte from peripheral blood mononuclear cells (PBMC) at
1194 10-week post infection by flow cytometry (F) MitoTracker Red in $CD115^{+}$ monocytes from
1195 PBMC at 10 weeks post immunization in uninfected and infected $ApoE^{-/-}$ mice. (G) Total cell
1196 counts from bone marrow cells utilizing trypan-blue discrimination of apoptotic cells (H)
1197 Percentages of CMP ($Lin^{-}CD127^{-}c\text{-}Kit^{+}Sca\text{-}1^{-}CD34^{+}CD16/32^{low}$) and GMP ($Lin^{-}CD127^{-}c\text{-}$
1198 $Kit^{+}Sca\text{-}1^{-}CD34^{+}CD16/32^{hi}$) (I) CMP cell counts in bone marrow $ApoE^{-/-}$ (J) GMP cell counts 10
1199 week post infection in $ApoE^{-/-}$ mice (K) Flow cytometry analysis of MDP defined as $Lin^{-}c\text{-}$

1200 Kit^{+}Sca-1^{-}FcγR^{low}CD34^{+}CD115^{+} (L) MDP cell counts in ApoE$^{-/-}$uninfected and infected male

1201 mice. Graphs are representative from experiments that were performed 3-4 times with n>4.

1202 Exception is MitoTracker data, which was performed twice, with n>4. Statistical analysis was

1203 done using unpaired Student's t test, *$p < 0.05$; **$p < 0.01$.

1204

1205 Figure 4.

1206 ***S. mansoni* infection induces sex-specific modulation of oxygen consumption and beta-**

1207 **oxidation in BMDM.** (A-C) oxygen consumption rate and spare respiratory capacity were

1208 measured at steady state. D-F) BMDM palmitate dependent oxygen consumption and spare

1209 respiratory capacity was measured in glucose limiting conditions. G) Oil Red O relative staining

1210 in BMDM from ApoE$^{-/-}$ mice (H) MitoTracker Red Deep Stain measure by flow cytometry in

1211 BMDM from ApoE$^{-/-}$ mice. SeaHorse assay analysis were performed the Seahorse XFe96

1212 instrument. *$p < 0.05$; **$p < 0.01$; ***$p < 0.001$. Graphs are representative of multiple

1213 experiments (2-3), with n>4 per group.

1214

1215 Figure 5**.**

1216 ***S. mansoni* infection induces significantly different cellular lipid profiles in BMDM from**

1217 **HFD female and male ApoE$^{-/-}$ mice.** A) PLS-DA derived score of LC-MS based lipidomic

1218 analysis of BMDM from HFD Infected females vs males. B) Box whisker plot of normalized

1219 AUC of cholesterol ester species, between female and male infected and uninfected HFD ApoE$^{-/-}$

1220 mice. C) PLS-DA derived score from Female HFD Infected and uninfected BMDM. D) Dot plot

1221 of lipid species identified in BMDM from infected and uninfected female ApoE$^{-/-}$ mice on HFD,

1222 significant lipid species are represented by red dots and labeled. E) Relative quantitation of BMP

1223 compounds in BMDM from male and female animals with and without *S. man*soni infection. F-I)
1224 Macrophages were differentiated with M-CSF in a 7-day culture with normal glucose and serum,
1225 and then switched to ^{13}C-labeled palmitate in dialyzed serum for 36 hours. J-N) Culture
1226 supernatants from BMDM stimulated with LPS for 24 hours were assayed for
1227 chemokines/cytokines. Data in A-E and J-N are representative of 2 biologically independent
1228 experiments with 4-8 mice per group. F-I are one experiment with 5-6 mice per group.
1229
1230

1231

1232 Figure 6.

1233 ***S. mansoni* infection differentially regulates the transcriptomes of BMDM from female and**
1234 **male ApoE$^{-/-}$ mice**. (A) Venn diagram showing upregulated genes in males only, independently
1235 of infection state and pathway analysis corresponding to the identified genes. (B) Venn diagram
1236 and pathway analysis of differentially expressed genes in males compared to females. (C) Gene
1237 ontology map of differentially expressed genes in response to *S. mansoni* infection in male
1238 compared to female ApoE $^{-/-}$ mice on HFD. Sequencing data are from one experiment with 5-6
1239 mice per group.

1240

1241 **Figure 7. *S. mansoni* induced modulation of male macrophage metabolism is long-lived in**
1242 **the absence of antigen.** Bone marrow from 10-week *S. mansoni* infected or control ApoE-/-
1243 mice on HFD was transferred into busulfan treated ApoE$^{-/-}$ recipients on HFD. A,B) Glucose
1244 tolerance test (GTT) at 10 weeks post-infection. GTT values were analyzed by Area Under the
1245 Curve and graphed using GraphPad Prism. C-E) Oxygen consumption rate and spare respiratory
1246 capacity were measured at steady state in 7day BMDM. F) MitoTracker Red Deep Stain measure

1247 by flow cytometry in BMDM. Data is two combined experiments 7-8 animals per group.

1248 Statistical analysis was done using Welch's t-tests.

1249

Figure 1

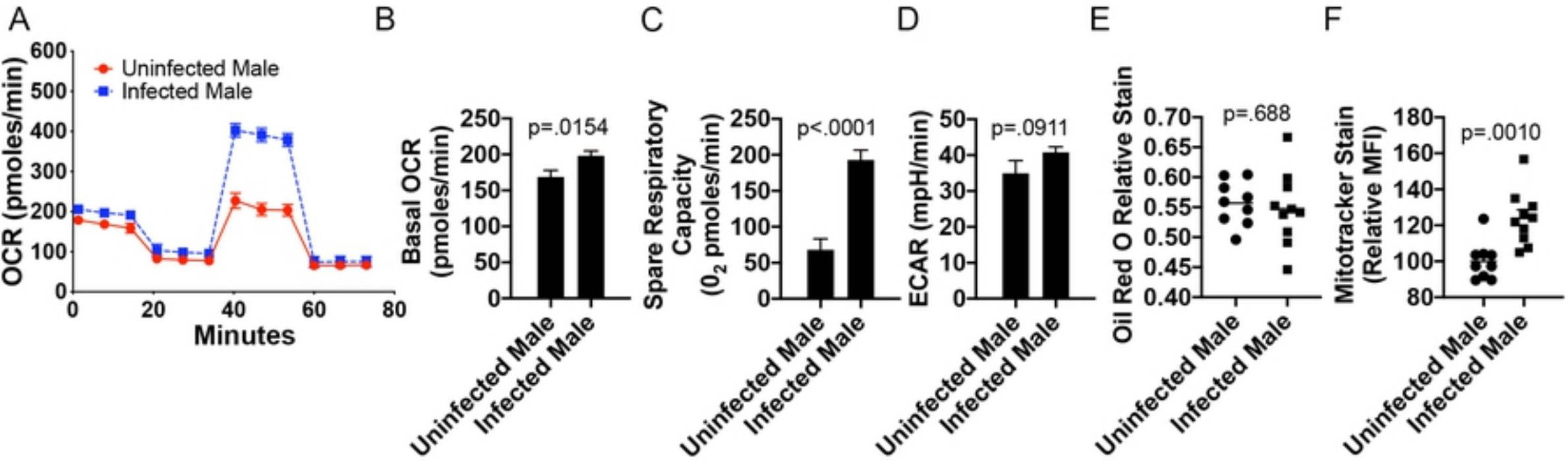

Figure 1

Figure 2

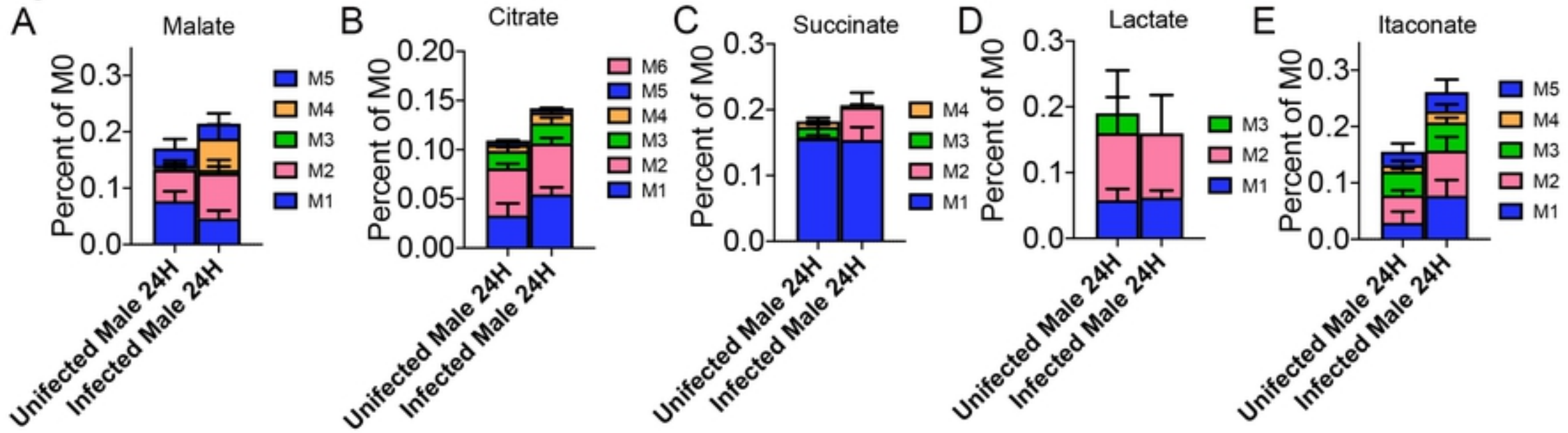

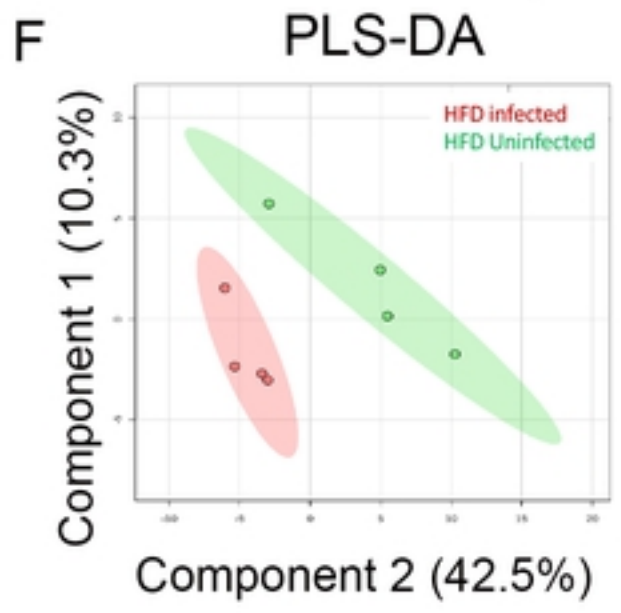

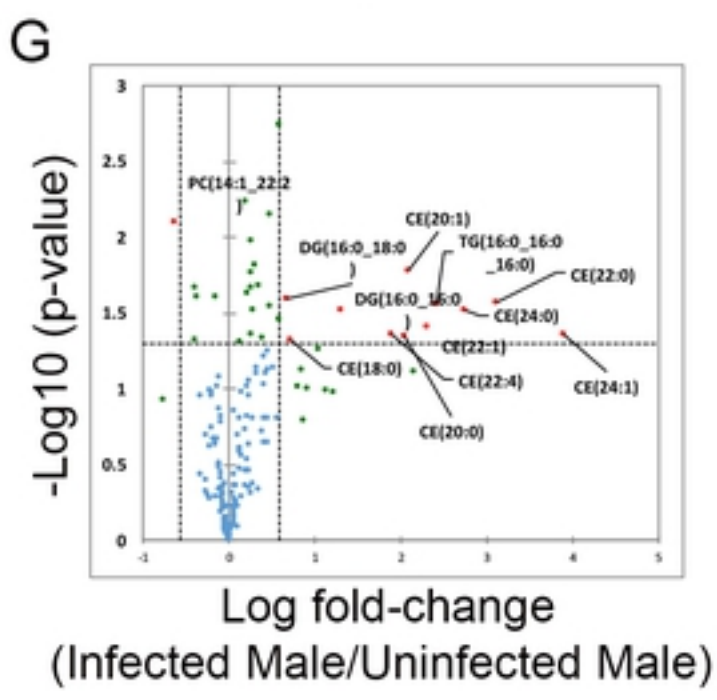

H

Name	Top ID	FC	log2(FC)	raw.pval	-log10(p)
CE_3048	CE(18:0)	0.61	-0.70209	0.047698	1.3215
CE_3259	CE(20:0)	0.24	-2.0498	0.045516	1.3418
CE_3025	CE(20:1)	0.24	-2.0828	0.01681	1.7744
CE_3388	CE(22:0)	0.12	-3.1123	0.027169	1.5659
CE_3239	CE(22:1)	0.20	-2.3098	0.039101	1.4078
CE_2793	CE(22:4)	0.27	-1.8932	0.044036	1.3562
CE_3458	CE(24:0)	0.15	-2.7462	0.030275	1.5189
CE_3378	CE(24:1)	0.07	-3.8946	0.043254	1.364
DG_2098	DG(16:0_16:0)	0.41	-1.2939	0.030364	1.5176
DG_2278	DG(16:0_18:0)	0.63	-0.67271	0.025481	1.5938
PC_1309	PC(14:1_22:2)	1.56	0.64476	0.0078633	2.1044
TG_2864	TG(16:0_16:0_16:0)	0.19	-2.4186	0.027936	1.5538

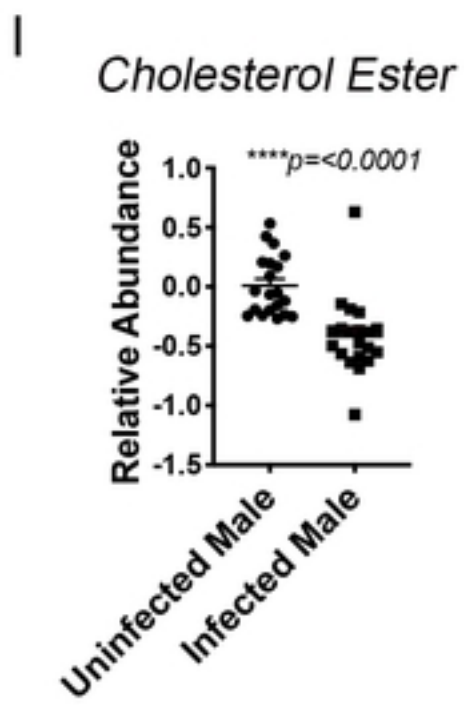

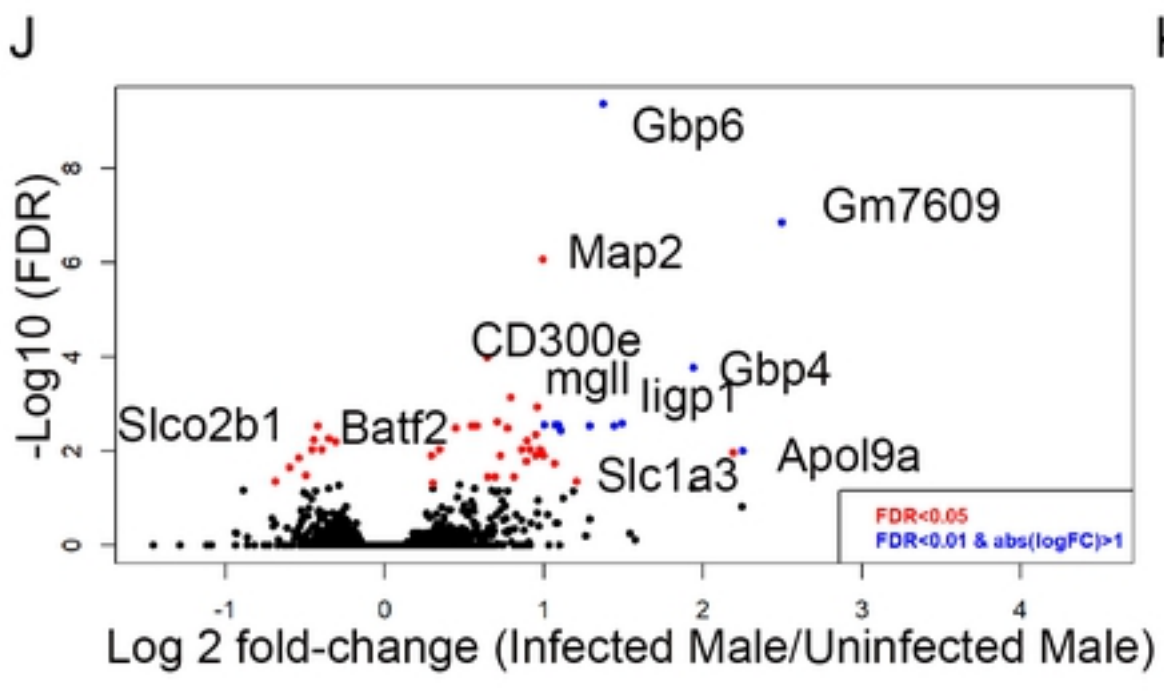

K

Pathway	P- value
Hematopoetic cell lineage	5.779E-08
Asthma	3.169E-05
Cytokine-Cytokine receptor interactions	0.0000894
Graft-versus host disease	0.0000894
Autoimmune thryroid disease	0.0000894
Type I Diabetes	0.0000894
Allograft rejection	0.0000894
Inflammatory bowel disease	0.0001406
Staphylococcus aureus infection	0.0001657
Cell adhesion molecules	0.0001722
Antigen processing and presentation	0.000212
Neuroactive ligand-receptor interaction	0.013
Phagosome	0.045

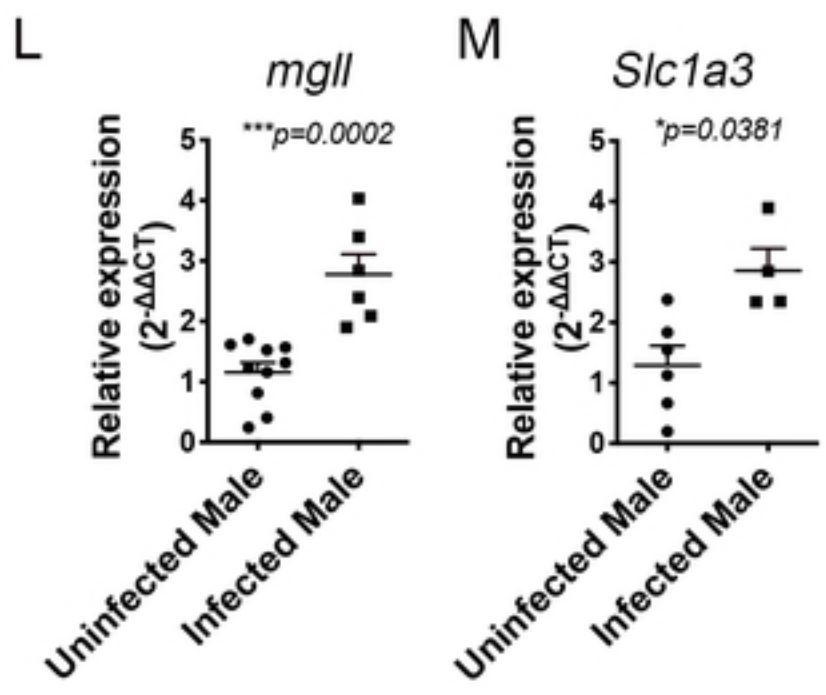

Figure 2

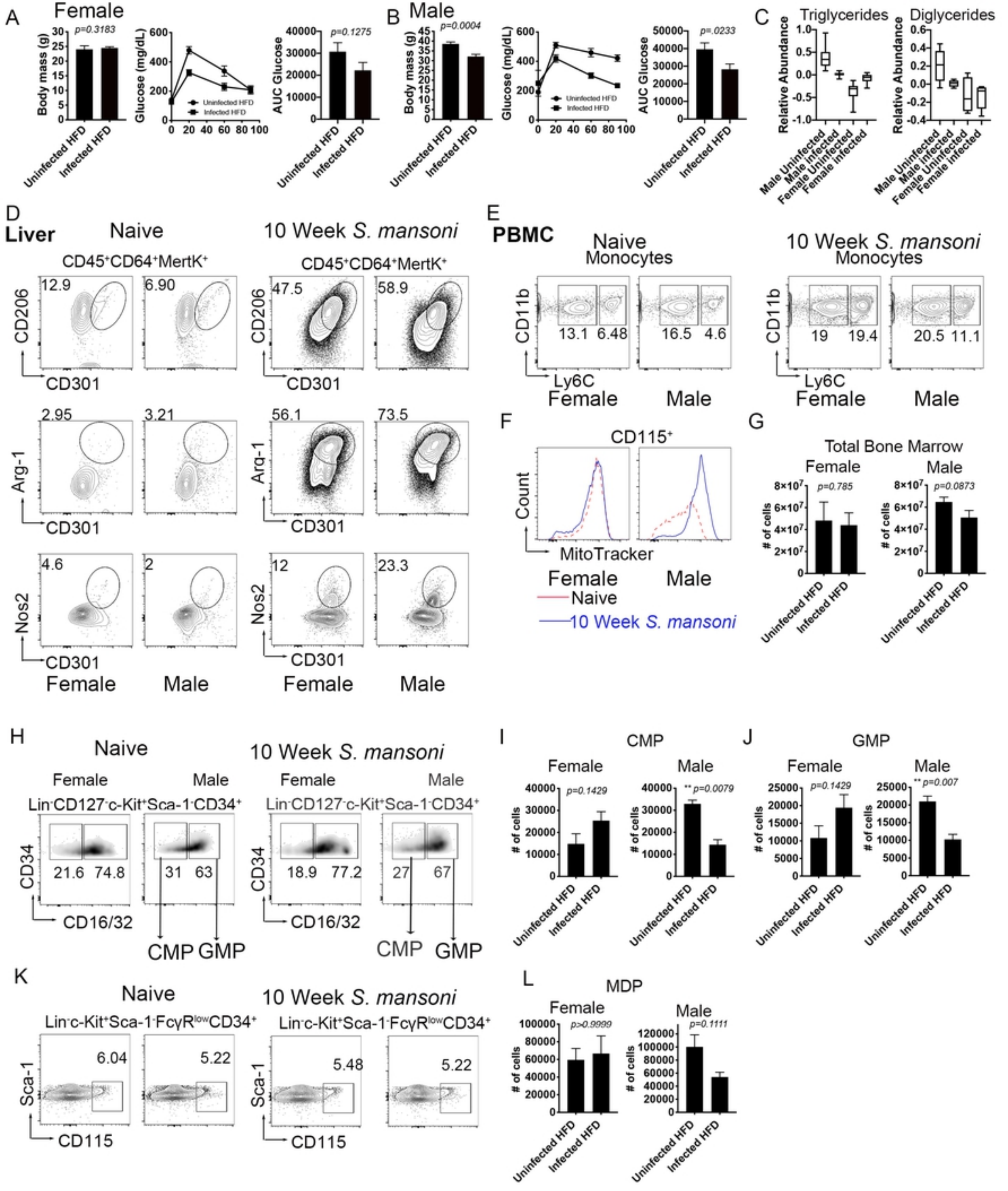
A
Female
Body mass (g)
p=0.3183
Glucose (mg/dL)
Uninfected HFD
Infected HFD
AUC Glucose
p=0.1275
B
Male
p=0.0004
p=.0233
C
Triglycerides
Diglycerides
Relative Abundance
Male Uninfected
Male Infected
Female Uninfected
Female Infected
D
Liver
Naive
10 Week S. mansoni
CD45+CD64+MertK+
CD206
CD301
Arg-1
Nos2
E
PBMC
Naive Monocytes
10 Week S. mansoni Monocytes
CD11b
Ly6C
Female
Male
F
CD115+
Count
MitoTracker
Naive
10 Week S. mansoni
G
Total Bone Marrow
# of cells
p=0.785
p=0.0873
H
Lin-CD127-c-Kit+Sca-1-CD34+
CD34
CD16/32
CMP
GMP
I
CMP
p=0.1429
** p=0.0079
J
GMP
** p=0.007
K
Lin-c-Kit+Sca-1-FcγRlowCD34+
Sca-1
CD115
L
MDP
p>0.9999
p=0.1111

Figure 3

Figure 4

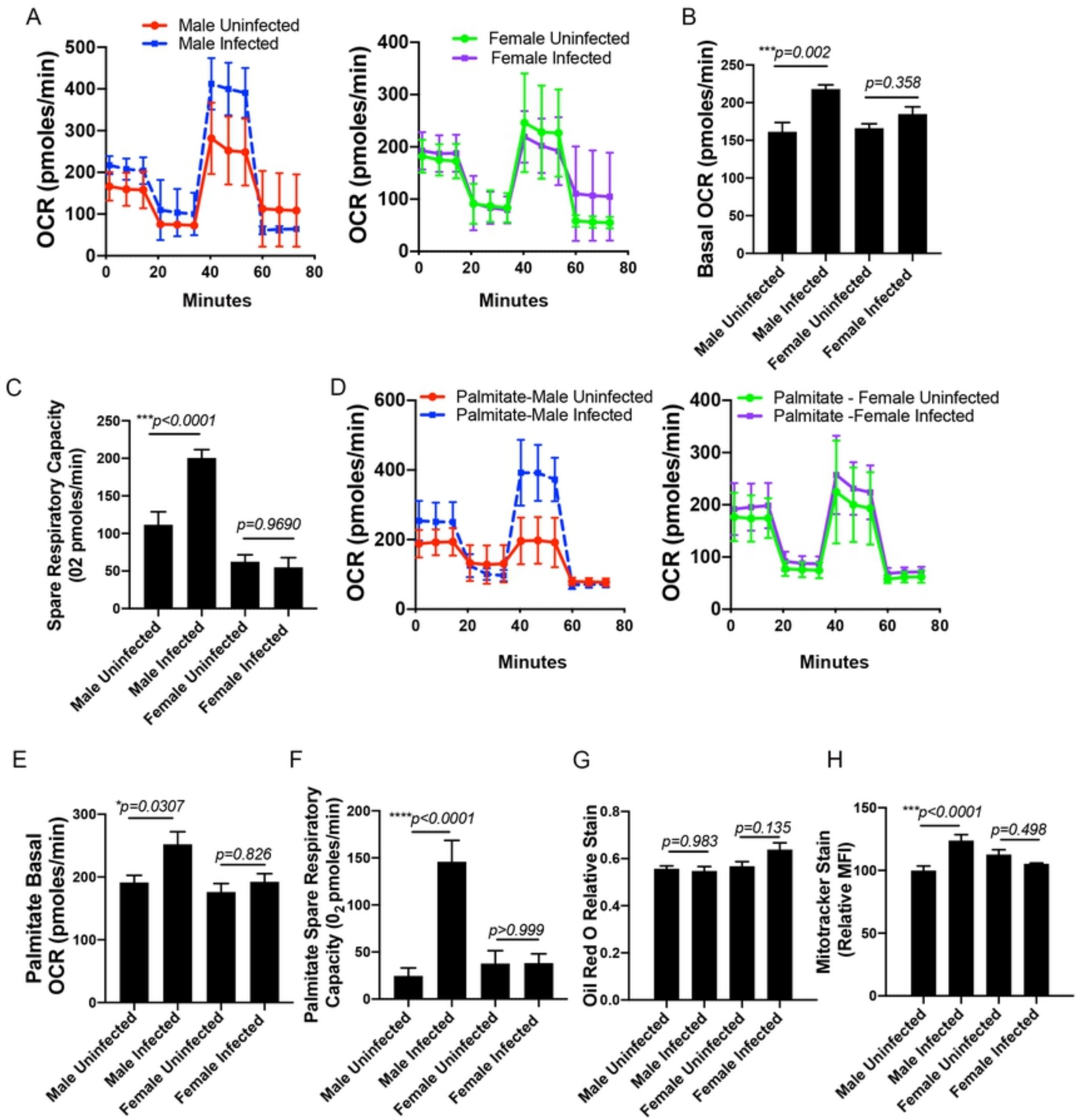

Figure 4

Figure 5

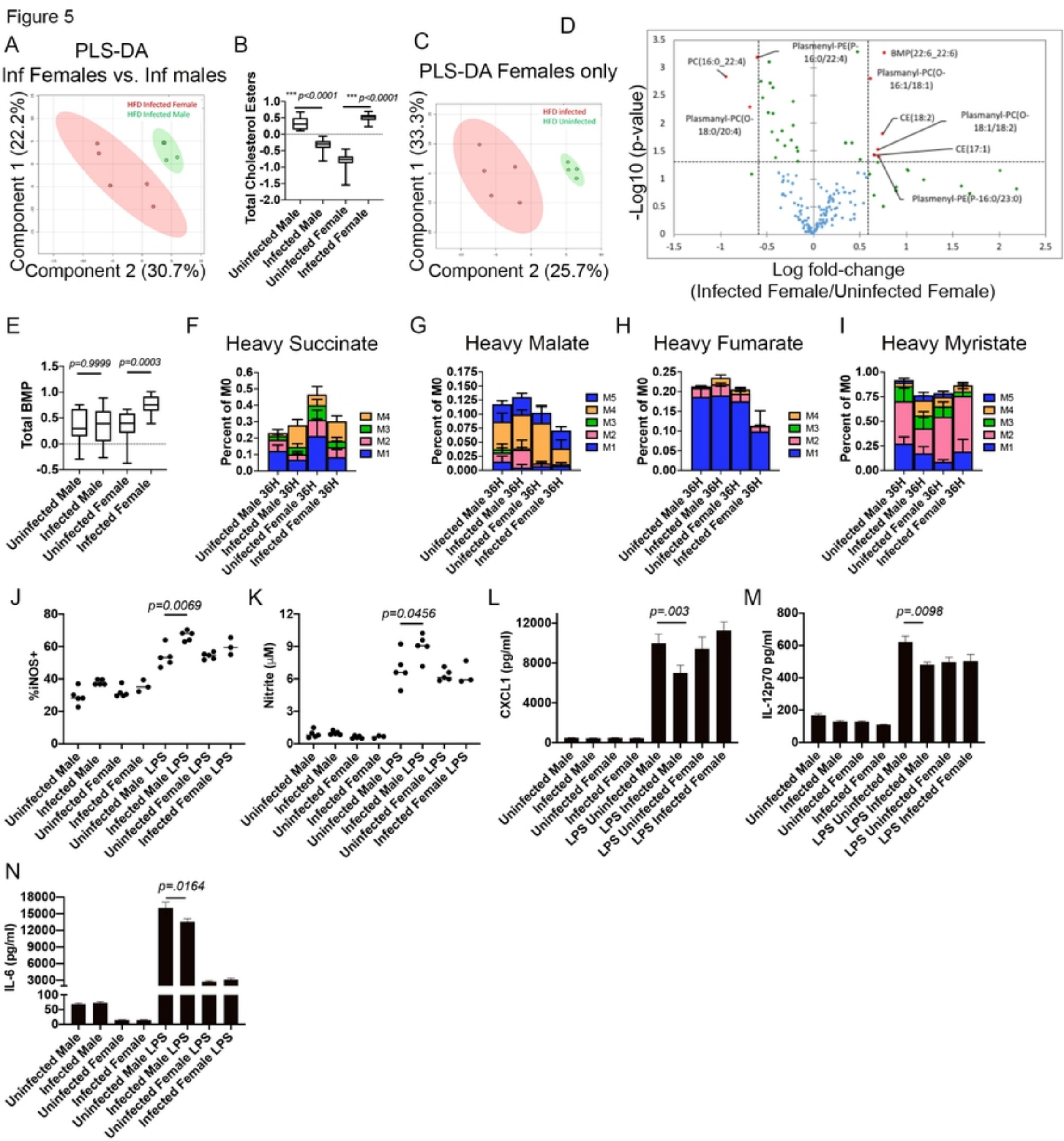

Figure 5

Figure 6

A Upregulated genes in males

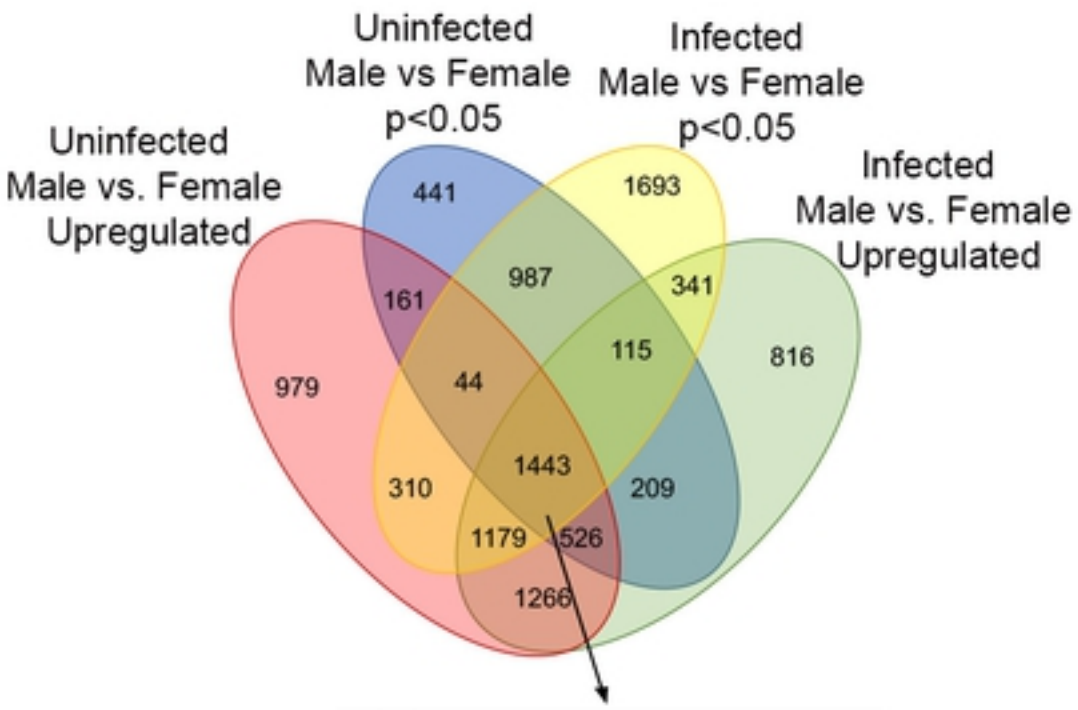

Pathways	Number of genes
Metabolism	238
Innate Immune System	216
Gene expression	183
Metabolism of proteins	149
Class I MHC Mediated Antigen Processing	85
Cell cycle	76
Vesicle mediated transport	72
Unassigned	63
Regulation of TP53 activity	52
NK-KappaB Signaling	47
DNA Double-strand break repair	42
Organelle biogenesis and maintenance	42
TNFR1 Pathway	31

B Differential regulation in male vs. female

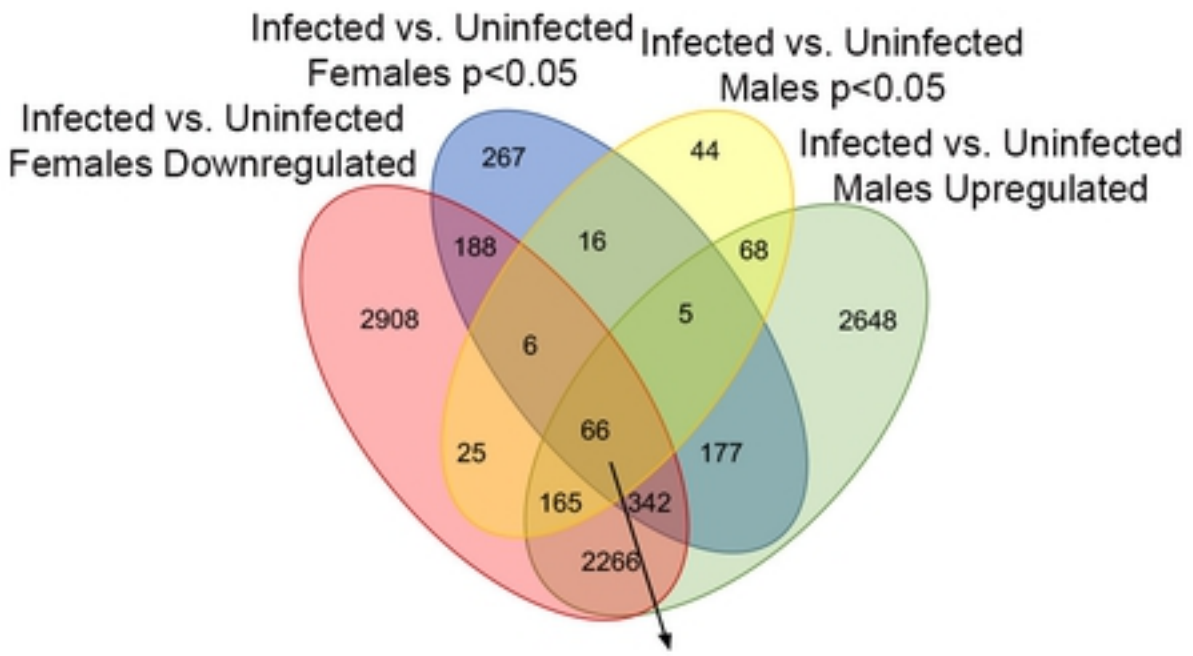

Pathways	Number of genes
Unassigned	31
Metabolism	10
Hemostasis	6
Adaptive immune system	2
Collagen degradation	2
Developmental biology	2
Metabolism of proteins	2
Neurotransmitter receptors and postsynaptic signal transmission	2
ROS and RNS production in phagocytes	2
Signal transduction	2

C Gene Ontology Map

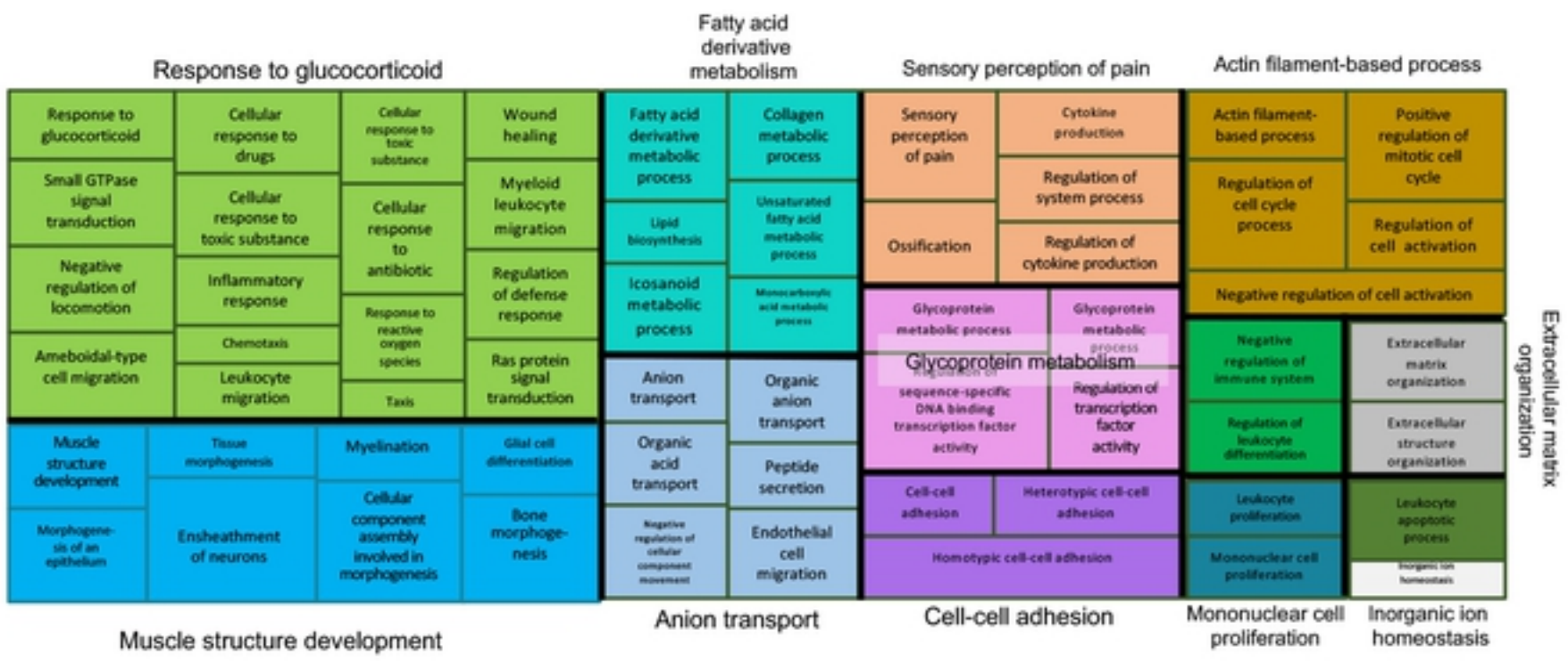

Figure 6

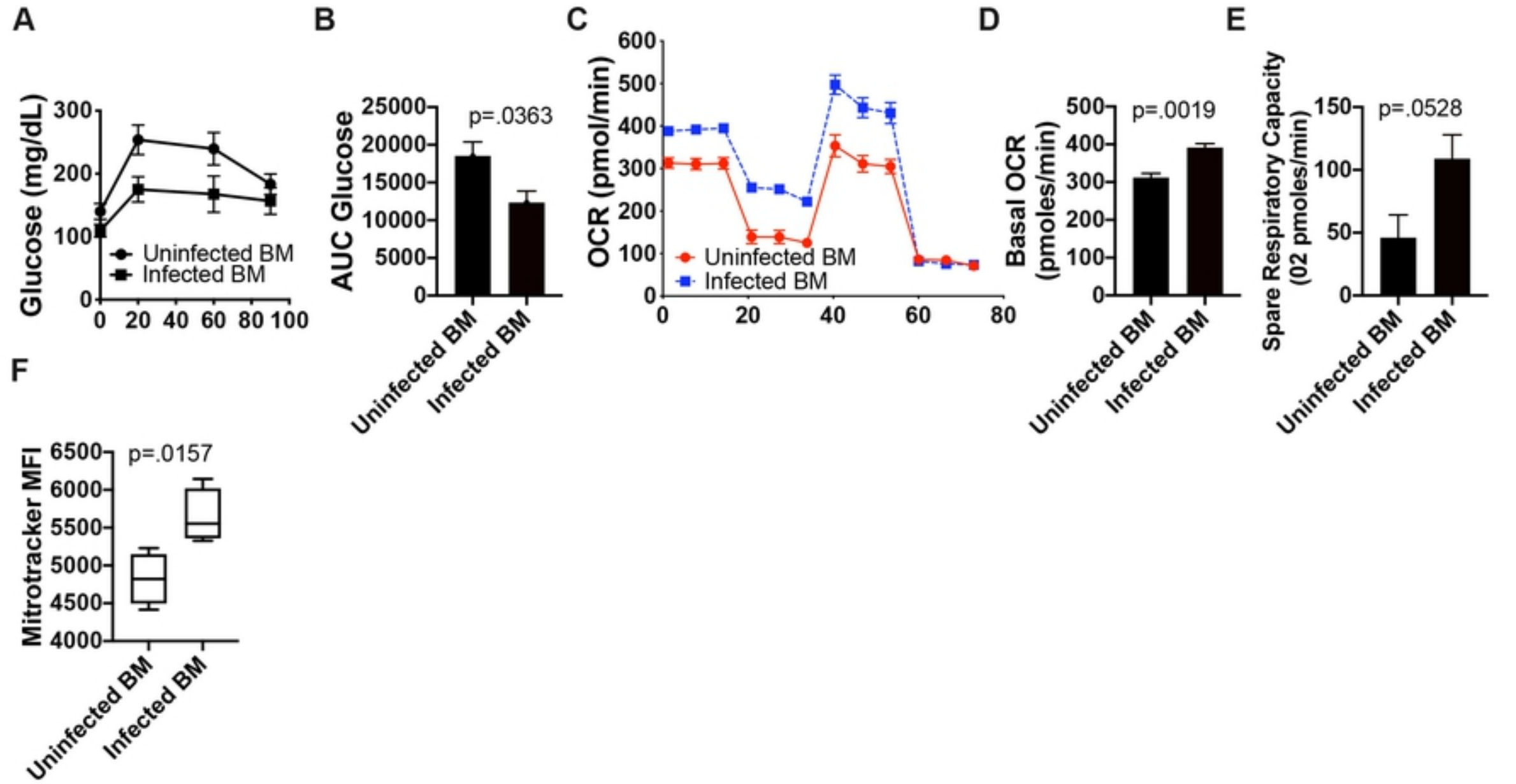
A
Glucose (mg/dL)
300
200
100
0
0 20 40 60 80 100
Uninfected BM
Infected BM
B
AUC Glucose
25000
20000
15000
10000
5000
0
p=.0363
Uninfected BM
Infected BM
C
OCR (pmol/min)
600
500
400
300
200
100
0
0 20 40 60 80
Uninfected BM
Infected BM
D
Basal OCR (pmoles/min)
500
400
300
200
100
0
p=.0019
Uninfected BM
Infected BM
E
Spare Respiratory Capacity (02 pmoles/min)
150
100
50
0
p=.0528
Uninfected BM
Infected BM
F
Mitrotracker MFI
6500
6000
5500
5000
4500
4000
p=.0157
Uninfected BM
Infected BM

Figure 7